The SIGNALS Legacy Survey
Science Justification

Context: In the past few decades, the astronomical community has expressed the need for integral field spectrographs (IFS) for conducting extragalactic science projects. Multiple instruments for the visible/near-IR have been and are still developed for this purpose, e.g. SITELLE, MUSE, SAMI, PMAS-PPAK[16,17,77,106]. By using these innovative instruments, several galaxy surveys have been performed while mainly focusing on one goal: acquiring a deeper understanding of galaxy evolution by studying their inner components in detail (e.g. SAMI survey[74], PHANGS, CALIFA). Notably the star formation and chemical enrichment processes were targeted as they are crucial ingredients in the interactions between stellar populations and the interstellar medium (ISM). More particularly, star formation also acts as a self-regulatory mechanism on the evolution of galaxies. Significant progress has been made in our global understanding of star-forming galaxies from these IFS studies. Nevertheless, at a spatial resolution of 60 to 1 000 pc, these surveys have had a limited impact in solving some of the physics of star-forming regions themselves as well as in establishing clear correlations between stars, gas, and galaxy dynamical structures. Either the spatial resolution was restricted by the sampling limit of the instruments (size of the fibers or pixels) or the field-of-view (FOV) was too small, forcing a selection of targets located at great distances. Therefore, the need for a high spatial resolution spectroscopic survey on larger, nearby star-forming galaxies remains (e.g. science case for the local volume mapper project of the next generation of the SDSS-V[73]). Designed for this purpose, CFHT's Imaging Fourier Transform Spectrograph (IFTS) SITELLE is the most efficient instrument to conduct such a survey. With its large $11' \times 11'$ FOV, SITELLE's spatial coverage is 100 times bigger than any competitor (see Tab. 3). Unlike fiber-fed systems, SITELLE gathers 100% of the light coming into the instrument with a much better spatial sampling ($0.32''$ per pixel) and improved blue sensitivity.

We propose to make use of SITELLE's unique advantages to conduct a detailed survey of star-forming regions in nearby galaxies. **SIGNALS**, the **S**tar formation, **I**onized **G**as, and **N**ebular **A**bundances **L**egacy **S**urvey, will be based on a **volume-limited sample of local extended galaxies ($D \leq 10$ Mpc) that are actively forming massive stars. It will provide the largest, most complete, and homogeneous database of spectroscopically and spatially resolved extragalactic HII regions ever assembled.** This will enable us to study small-scale nebular physics and many other phenomena linked to massive star formation in galaxies at a mean spatial resolution of ∼20 pc. Our sample includes ∼40 spiral and irregular galaxies. HII regions present a wide variety of characteristics: morphology (from compact to extended shells), mass (where the low luminosity regime is not very well sampled), metallicity (where the rare metal-poor regions have been less studied), or age (following the diversity of their young stellar populations). They may be located in different galactic ecosystems and coexist with other sources of ionization (like shocks and AGN). This volume-limited sample will provide a statistically reliable laboratory, with over 50 000 resolved HII regions.

HII regions are at the heart of this proposal and the large sample proposed will be an order of magnitude greater than the state-of-the-art dataset currently available. By studying the spectra of spatially-resolved individual HII regions and their massive star content, SIGNALS aims for understanding how diverse local environments (nearby stellar population mass and age, gas density and chemical composition, dynamical structures, etc.) affect the star formation process.

The legacy of our survey will reflect on many topics in astrophysics, from stars to very distant galaxies. Our primary immediate goals are to :
1) quantify the impact of the near surrounding environment on the star formation process,
2) link the feedback processes to the small-scale chemical enrichment and dynamics in the surrounding of star-forming regions, and
3) measure variations of the resolved star formation rate with respect to indicators used for high-redshift galaxies.

This document presents the SIGNALS project under four sections addressing its main scientific themes: star formation process, feedback mechanisms, small-scale dynamics, and the influence of the local environment. While these topics are all interconnected, this subdivision provides a structure to navigate throughout the different angles of attack needed to study the small-scale physics of star-forming regions and to understand the impact of their close environment. A good example of the complexity and intricacy of these mechanisms can be seen in the spectacular dataset we have recently obtained for the nearby spiral M33 under joint Canada-France-Hawaii PIs' proposals. Figure 1 shows a mosaic of the inner portion of M33 produced with four SITELLE pointings and the three filters SN1, SN2, and SN3 (covering the main emission lines). The sensitivity, spatial coverage, and resolution are exceptional and clearly demonstrate the observational strategy needed to address the scientific goals as stated for SIGNALS.

A Star Formation Process at the Scale of an HII Region

HII regions are non-uniform bubbles of ionized gas found in the surrounding of young stellar clusters (YSC) containing one or more massive-ionizing OB stars[91]. They are ideal laboratories to study star formation process at a moderately-early stage before an age of 40 million years. They are optically thin in the visible light; emission from both the stars and the gas is accessible. Their sizes vary from one to a few hundred parsecs depending on their massive star content, their age, and the density of the circumstellar medium[91]. The slope of their Hα luminosity function and their size are known to vary between galaxies, but the physical explanation for these discrepancies remains unknown[5].

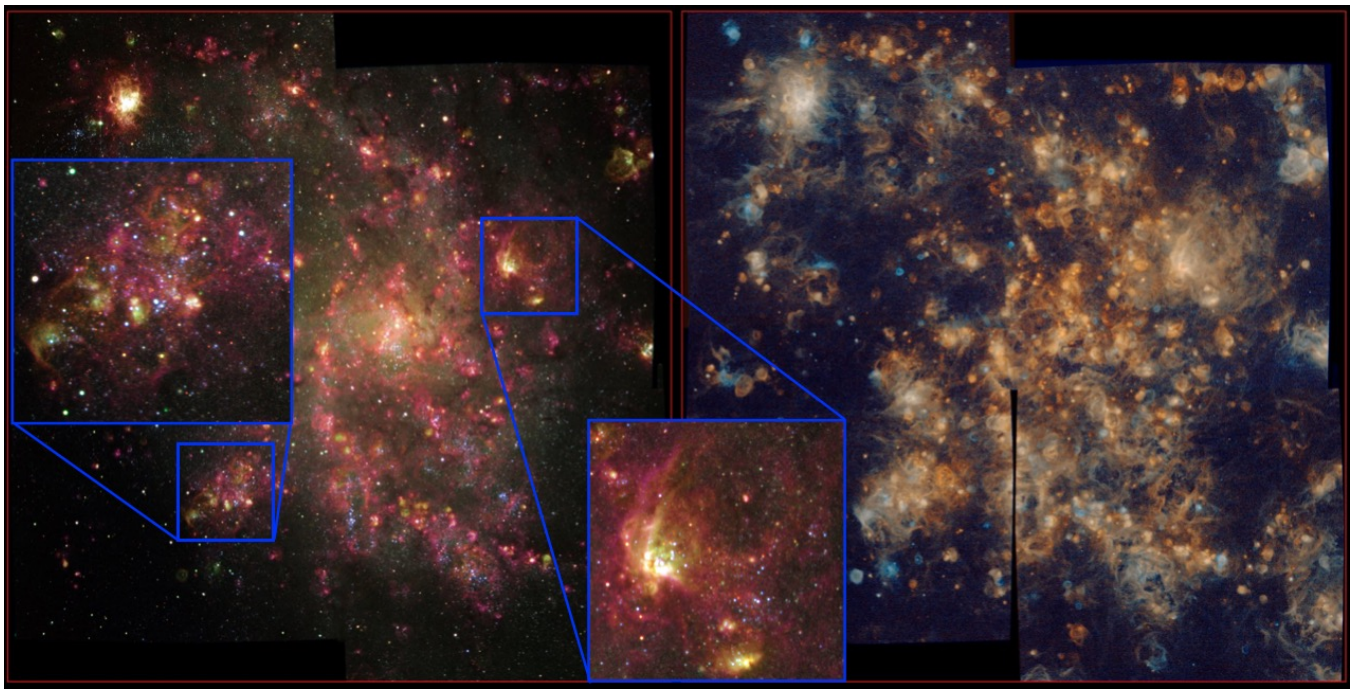

Figure 1: On the left, composite image of M33 using three filters, combining for each filter the flux over the full wavelength range plus one emission line: SN3+Hα (red), SN2+[OIII]λ5007 (green), and SN1+[OII]λ3727 (blue). On the right, the emission line map of Hα, [OIII]λ5007, and [OII]λ3727 using slightly different shades of orange, green, and blue respectively.

Among the HII region population, variations in mass, brightness, and spatial extent are not fully understood. Moreover, possible differences in their stellar initial mass function (IMF) have been reported in some cases[113]. Although it has been proposed that these variations could be related to the location of the HII regions in different galactic structures (e.g. bar, arm, and inter-arm environments) or the fractal morphology of the ISM on the scale of $\sim$100 pc[38], the physics behind this explanation is still unclear. What influences these characteristics in the close environment of an HII region? To get an insight on the small-scale physics involved in the star formation process, one needs to dissect many star-forming regions and study them individually in their environmental context.

A.1 Star Formation Rate and Resolved Star Formation Law

The star formation rate (SFR) is a fundamental cosmological parameter in our understanding of galaxy evolution in the Universe. Indicators of the SFR such as the integrated Hα, [OIII]λ5007, or [OII]λ3727 luminosity are frequently used in the literature for both low- and high-redshift galaxies[66,89]. Nevertheless, the accuracy of these indicators depends on the relation between the HII region gas emission and the total mass of their YSC. Therefore, possible variations of the IMF or the gas metallicity through cosmic time could result in significant errors on SFR determined from these indicators, because of the changes of the gas emission to stellar mass ratio. One way to track these effects on the integrated flux of the gas emission lines is to establish the HII region luminosity function. The luminosity function is built from resolved and complete HII region populations with different masses, metallicities, and environments. Therefore, observation with high spatial resolution are required. Also, to accurately establish the shape of the luminosity function, a large number of regions must be considered ($\sim$1 000[107]), and numerous physical conditions must be studied (metallicity and environmental parameter bins; e.g. stellar density, star formation efficiency).

To separate individual HII regions, a spatial resolution of a few tens of parsecs is required[73]. Figure 2 illustrates how the ionized gas structures and individual clumps of star formation can be resolved while increasing the spatial resolution. Below a resolution of 50 pc, observations reveal structures in the ISM including individual star-forming knots, diffuse ionized gas (DIG), and shocks. Figure 2 (on the right) shows the impact of the spatial resolution on the detection of HII regions in a small portion of the spiral NGC628 observed with SITELLE during the science validation phase. Our identification algorithm is able to detect $\sim$8 times more HII regions when the resolution improves from $\sim$100 to 35 pc. This figure compares the same regions observed with SITELLE ($\sim$0.9″) and (SITELLE's prototype) SpIOMM ($\sim$3″); while 566 regions have been detected with SpIOMM, we were able to detect 4285 with SITELLE[107,108].

As mentioned above, our analysis of the science verification data allowed us to identify 4285 HII region candidates in NGC 628 using a tailored procedure developed for the SITELLE data at a spatial resolution of 35 pc[107]. Our procedure uses two advantages of the IFTS: the full spatial coverage and the spectral information. By combining the flux of three emission lines (Hα, Hβ, and [OIII]λ5007), we increased the detection threshold and improved the detection of the low metallicity regions with much fainter recombination lines. This code provides flexibility in defining regions and their DIG background. Our method proceeds through multiple steps: 1) identification of the emission peaks, 2) determination of the zone of influence around each peak, and 3) definition of the outer limit of a region and its DIG background. These operations are done without any dust extinction correction to avoid introducing unnecessary noise. Figure 3 shows the border of a few HII region derived with this procedure; it will be adapted to different spatial resolutions to make sure that the regions are uniformly defined.

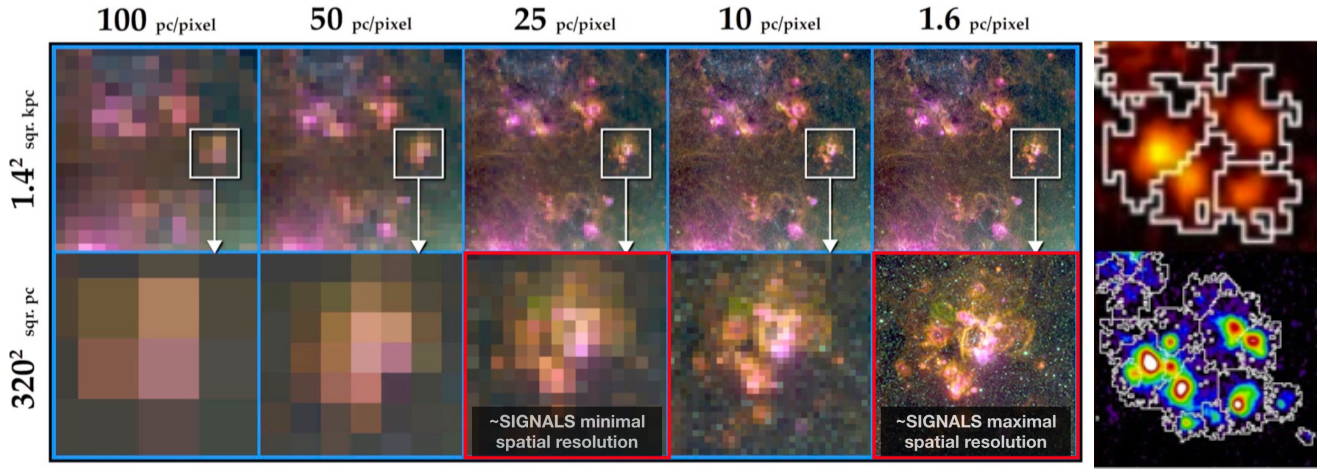

Figure 2: On the left, the impact of the spatial resolution on resolving the ionization structures of the ISM[107][73]. Note that SIGNALS (seeing-limited) minimum spatial resolution is slightly better than the sampling-limited 25 pc/pixel case, and the maximal resolution is slightly better that the sampling-limited 1.6 pc/pixel case. On the right, the impact of the spatial resolution on the detection of the ionizing sources and emission line regions is shown. At the top, an Hα image from SpIOMM of a complex of HII regions in NGC 628 (3.0″ seeing, 1.1″ pixels, resolution ∼100 pc). At the bottom, the Hα image from SITELLE of the same complex of HII regions (0.9″ seeing, 0.32″ pixels, resolution 35 pc).

Among other things, the SITELLE's dataset for NGC 628 was also used to recover the luminosity function for different samples of HII regions as shown in Figure 4. These luminosity functions are derived using 2000 - 4000 regions at a time and are very well defined. These results are extremely promising and show that a resolved star formation law will be within reach of the SIGNALS project. **By spatially-sampling HII regions properly, and by studying the impact of the metallicity, IMF variations, and the possible local environment influence on the luminosity function, we will provide the community with SFR indicators adapted for specific science cases.**

A.2 HII Region Physical Characteristics

SITELLE's hyperspectral datacubes allow us to not only properly sample HII region luminosity functions, but also to characterize the ionized gas properties and gather information on the region environment. Each HII region is a peculiar beast. The emission of the various recombination and collision lines along with the global shape of the nebulae might be different depending on the spectrum of the ionizing source, on the density, homogeneity, and chemical abundances of the gas, as well as on the interaction between the population of free electrons and ions present.

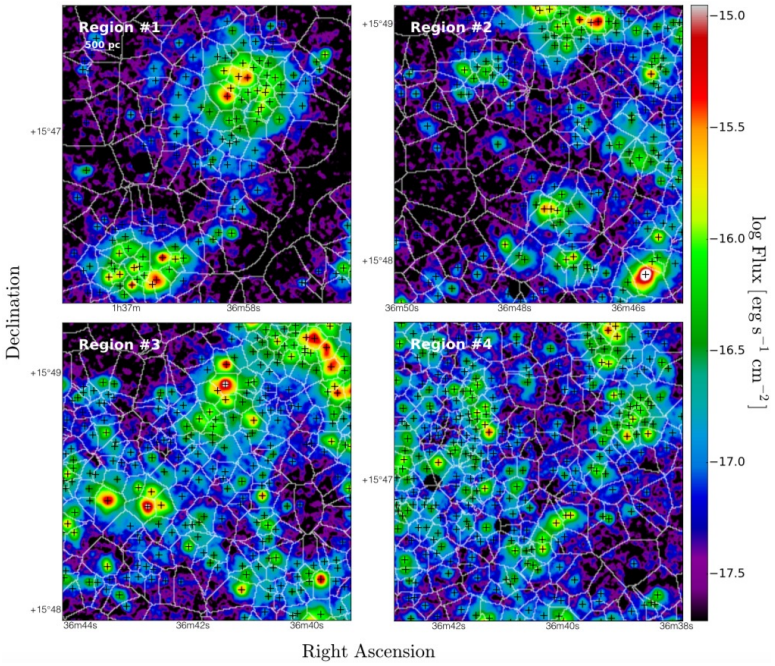

Figure 3: Examples of ionizing sources and their zone of influence in NGC 628 drawn over the Hα+Hβ+[OIII]$\lambda\lambda$4959,5007 continuum-subtracted image. The location of the four reference regions may be seen on the Hα image in Figure A2 of Rousseau-Nepton et al. [107]. The centroid position of each emission peak detected is identified with a cross. The white contours define the zones of influence surrounding the emission peaks.

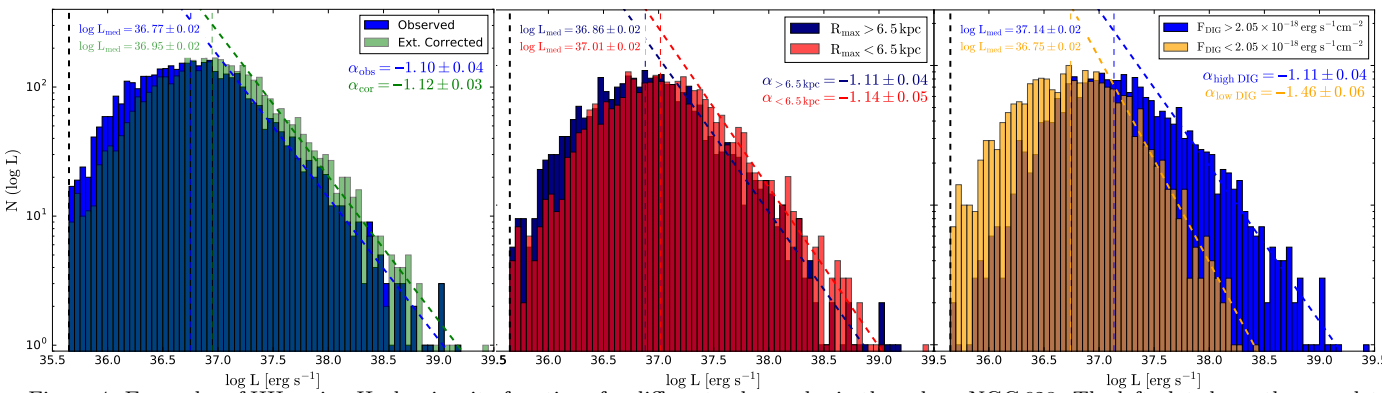

Figure 4: Examples of HII region Hα luminosity functions for different subsamples in the galaxy NGC 628. The left plot shows the complete sample before and after the dust extinction correction. The other plots show the HII regions divided in two equal subsamples with respect to the galactocentric radius (middle plot) or the DIG background level (right plot) as measured for each region.

As the HII region characteristics are all related to each other, modeling the photoionization conditions is the best method to reconnect observations to the physical conditions. SIGNALS will reveal unique information about the gas abundances, density, filling factor, stellar content, and the fraction of ionizing photons escaping nebulae. On top of being used to categorize the regions selected to define the luminosity functions, these parameters will be compared to environmental elements such as the DIG background, the neutral gas density, stellar populations, the velocity dispersion, and the local mean abundances. This will provide unique insights on feedback mechanisms, chemical enrichments, and small-scale mixing.

A.2.1 Gas Conditions, Photoionization, and Ionized Gas Models

Metallicity, Abundances, and Spectral Energy Distribution of the Ionizing Sources - Photoionization models are essential tools to understand the physical properties of HII regions whether or not the ionization structure is resolved, e.g. CLOUDY[43,88] or MAPPINGS[34,56]. With SITELLE's spatial resolution, we can use multi-dimensional photoionization models in order to precisely constrain gas properties of HII regions[124,126,127]. Figure 5 shows examples of the structures seen in the ionized gas mapped with the [OII]λ3727/[NII]λ6583 line ratio in specific regions within NGC 628. For each source detected, we establish a mean profile of all line ratios as a function of the distance to the ionization source (OB stars in the case of HII regions). These profiles along with the integrated flux of each line are needed to conduct a fair comparison with models. The spatial resolution and filling fraction of the observations are also important for analyzing the photoionization conditions. Figure 6 shows the impact of the FOV and filling-factor on the HII region spectrophotometry by comparing the log [NII]λ6583/Hα maps obtained with SITELLE and the CALIFA PPAK IFU survey (filling factor ∼60%[103]). The maps differ significantly. This comparison reveals sampling difficulties facing surveys at lower spatial resolution when analyzing the ionized gas emission[48,102]. Notably, for fiber-fed systems, 1) the flux of faint areas covered by fibers become negligible resulting in a global flux dominated by the brightest area and, 2) areas not covered by fibers no longer contribute to the resulting map and therefore some important structures might be difficult to identify.

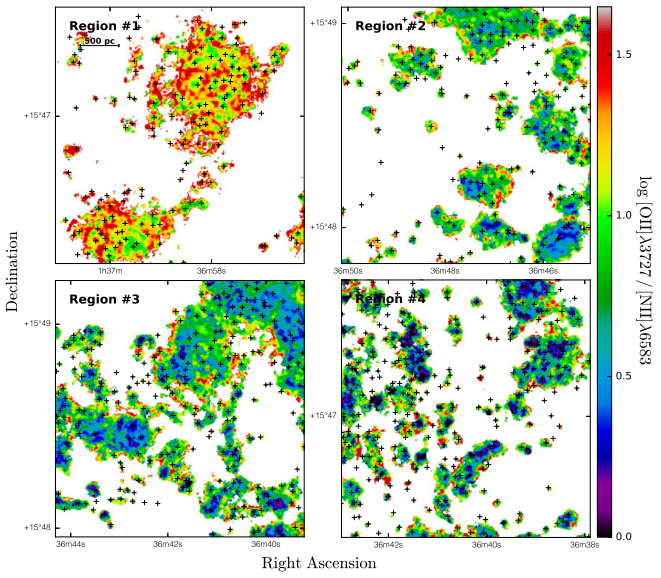

Figure 5: Examples of the ionized gas structures from the [OII]λ3727/[NII]λ6583 line ratio map over four areas of the galaxy NGC 628. The location of the four regions may be seen on the Hα image in Figure A2 of Rousseau-Nepton et al. [107]. The centroid position of each emission peak is identified with a cross. The value of the line ratio changes as the distance from the peak increases.

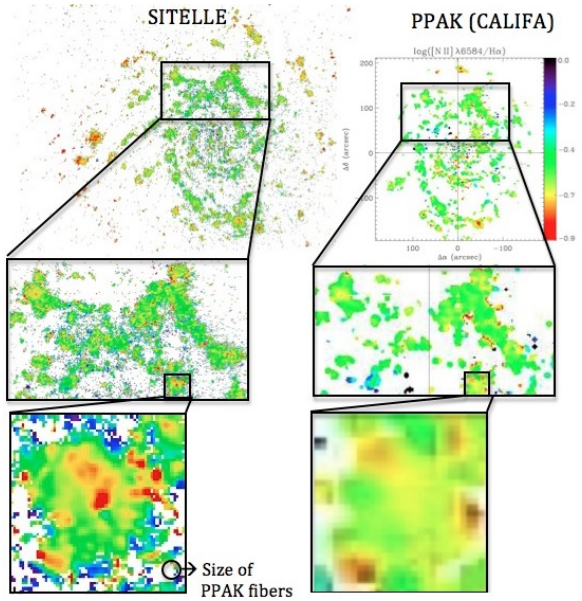

Figure 6: Spatial resolution and filling factor impact on the measurements of emission line ratios. Log [NII]λ6583/Hα line ratio extracted from SITELLE's observations on NGC 628 (0.8″ seeing, 0.32″/pixels, 100% filling factor) compared to PPAK's observations on the same area (0.8″ seeing, 2.7″/fiber, 60% filling factor). The color scale is the same for both maps (upper-right corner).

We already have in hands grids of models of HII regions with different properties from various photoionization codes (BOND[120], 3MMdB[88], and MAPPINGS) to compare to our data. These grids are designed to study the effect of variations in the gas conditions on the integrated spectrum (region by region). Figure 8 shows an example of the comparison of emission line ratios observed in NGC628[107] with integrated values obtained with BOND. Additionally, we can compare with 1D models the 2D structure of the resolved HII regions pixel by pixel. Figure 7 shows a comparison of four line ratios with a 1D model extracted with CLOUDY. Different photoionization parameters can account for variations in the spectral energy distribution (SED) of the source, the metallicity, and the relative abundances of elements. The ionizing source can be one or many massive stars, a stellar population template (with different age, IMF, and metallicity), or any peculiar object. The model performance can be improved by comparing results with a set of regions for which the ionization sources have been observationally constrained. In particular, we plan to develop a synergy between SIGNALS and the Legacy ExtraGalactic UV Survey (LEGUS). LEGUS is a Treasury Program of the Hubble Space Telescope (HST) that will image 50 local (<12 Mpc) galaxies in multiple filters from the UV to the visible (see Tab. 3). Because of the proximity of all LEGUS targets and the HST spatial resolution, the galaxies are resolved into their main components: stars, star clusters, and associations. Therefore, we will build templates of

the YSCs using the flux in the different bands available from both SITELLE (SITELLE deep frames correspond to ∼U, V, and R) and HST, and combine the SED of these sources with photoionization codes, while simultaneously accounting for the dust extinction effect on the Balmer lines, to reproduce the observed emission lines from the gas. The combined information from SIGNALS and LEGUS will provide a complete view of the HII region physics for a large fraction of our galaxy sample. The LEGUS data products include a catalog of young cluster characteristics for a few galaxies[1,51]. This catalog provides the position, mass, and age of the clusters. Associating a SIGNALS HII region with a LEGUS cluster will therefore be facilitated.

We will constraints existent photoionization models using several line ratios simultaneously. Ratios available within our dataset are listed in Table 1 of the Technical Justification. The combination of these line ratios will allow us to cover a broad range of physical conditions for the gas and the ionizing source. Some line ratios are more or less sensitive to variations in metallicity, depending on the metallicity regime of the regions[70,94,120]. This is one of the main aspects that drove the selection of the filters for our program. SITELLE's high sensitivity in the blue enables the detection of the [OII]λ3727 lines, essential to accurately determine ionized gas properties[68,83] in some ionization or metallicity regimes. With all the lines available, SIGNALS' multi-dimensional analysis of HII regions will give us an unprecedented view of the metallicity distribution in the ISM of nearby galaxies.

We will investigate variations of abundances on the scale of a few parsecs. Local variations can reveal the mixing time-scale[95] with respect to the main galactic structures and dynamical properties of the ISM. **Such a detailed analysis has never been performed on a vast sample that includes tens of thousands of HII regions. In addition to the region by region analysis, a statistical approach will be used to study the HII regions' distribution.** Figure 9 shows simulations of line ratios when combining photoionization models with evolutionary tracks of star-forming clusters.

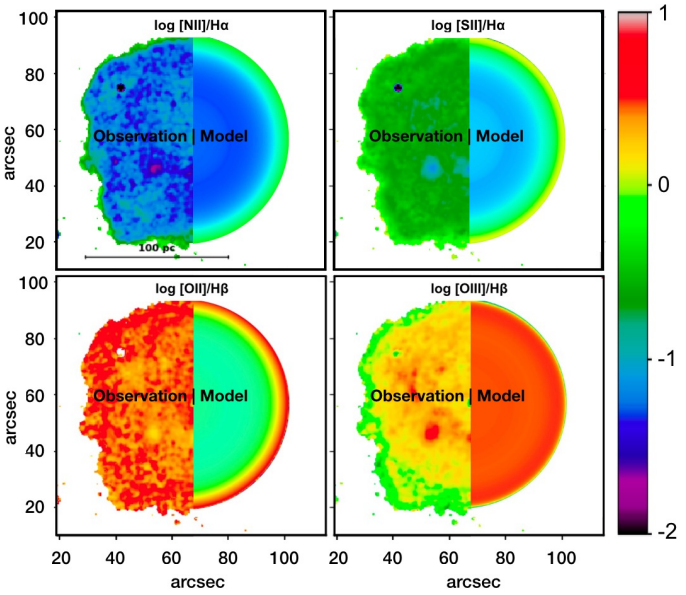

Figure 7: Comparison of a giant HII region in NGC 6822 with a 1D photoionization model (Co-I Heidelberg). The region is split in two: the left side is the 2D observation while the right side is the 1D model (a slice perpendicular to the line of sight that goes from the center of the region to the outskirts). Depending on the brightness of the lines with respect to the distance to the center, the integrated spectrum through the line of sight reflects the integrated value of the model. For example, the observation of the line ratios [NII]λ6583/Hα and [OIII]λ5007/Hβ allow to see through the ionized bubble whereas the [SII]λ6583/Hα and [OII]λ3727/Hβ ratios are dominated by the value on the expanding-ionized shell (at the ionizing front).

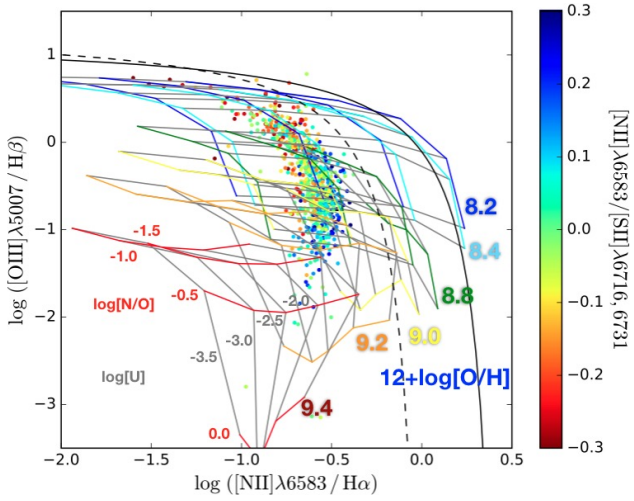

Figure 8: BPT diagram[6] of emission line regions identified in NGC 628[107] along with a grid of models from BOND[120] using the SED of a 3 Myr old YSC with a Chabrier IMF[26]. The grids' colors identify the different metallicities (12+log[O/H]). The different values for log[N/O] follows the colored lines (shown in red for 12+log[O/H] of 9.4), and log[U] follow the grey lines (shown in gray). The color-scale of the scattered observational points indicates the log[NII]/[SII]λλ6716+6731 line ratio known to be a good indicator of log[N/O][94]. The limit between the HII regions and the transition regime[65] is shown by the dashed curve, and the extent of the starburst domain[69] by the continuous curve.

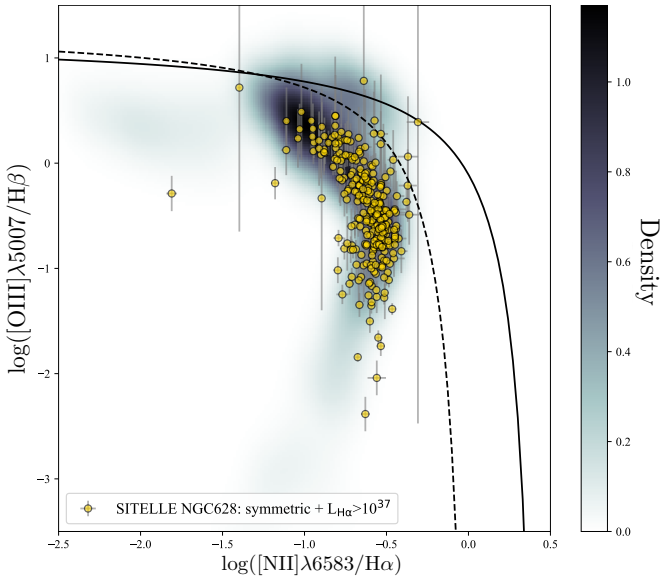

Figure 9: BPT diagram[6] of emission line regions identified in NGC 628 in Rousseau-Nepton et al. [107] (using symmetric regions only) along with simulations from CLOUDY using post-processing of evolutionary tracks from the WARPFIELD code[100]. It combines a series of WARPFIELD runs with different cloud masses, densities and ages, the color-coding indicates the relative number of model outputs producing a line ratio. See Figure 8 caption for the curves definitions.

The code WARPFIELD[101] (Winds And Radiation Pressure: Feedback Induced Expansion, colLapse and Dissolution) EMP (Emission Measure Predictor) was used to produce the Figure 9. WARPFIELD is a new semi-analytic model

to describe the impact of mechanical and radiative feedback from a young massive cluster on its parental cloud. Our approach simultaneously and self-consistently calculates the structure and the expansion of shells driven by feedback from stellar winds, supernovae, and radiation pressure, while accounting for the deceleration of the shell due to gravity. The model has been used to investigate the conditions in which the different sources of feedback dominate and the amount of radiation that escapes through the shell, and to derive minimum star formation efficiencies for a large parameter space of clouds and clusters[101]. The same approach was used to explain the two stellar populations in NGC 2070 in the LMC, which hosts the younger cluster R136 in its center[100]. Because this method is computationally very efficient, it will allow us to consider a large range of parameters and we are currently building up a comprehensive database in which we vary the star formation efficiency, the cloud mass and density profile, and the metallicity of both the gas and the stars. Each model is currently being post-processed using CLOUDY code to make detailed predictions for the time evolution of the line and continuum emission associated with the system. We can build synthetic BPT-like diagrams for the one-to-one comparison with observational data, as shown in Figure 9.

As mentioned previously, there is a strong link between the shape and emission of a region and the ionized gas conditions (especially the metallicity, density, and porosity), the massive star content and age, the interaction with the local ISM (molecular clouds or DIG), and the local radiation background (stars, AGN, etc.). Nevertheless, all these elements cannot be included at once in a comprehensive grid of models to study a region. Therefore, by combining UV, HI, and CO data for some targets, a subset of the SIGNALS data will be used to complete our analysis of these aspects (Section A.2.2 and A.3). We are aware of the difficulties related to the entanglement of the HII regions physical characteristics and the modeling of the emission line spectrum that contains only a limited amount of information. The SIGNALS' team will work on this aspect with great care. The vast sample of HII regions will help us with this task and we will be in the best position to overcome this issue.

A.2.2 Massive Stars Content and IMF Variations

Mass, Age, and SFR - From the number of parameters involved in the study of HII regions, one cannot exclude the possibility that the IMF changes within different environments. It is also impossible to infer two distinctive modes of massive star formation (competitive accretion vs isolated gravitational core-collapse) without supposing that the global IMF of the stellar populations in a galaxy could be affected. The IMF of massive stars has an impact on the determination of the mass and age of the YSC which is essential for deriving a resolved SFR. To determine these parameters along with the extinction coefficient Av, many have compared photometric observations (in different bands) with stellar population models[115,125]. However, these photometric techniques are affected by contamination from the gas emission (emission lines and continuum), underlying old clusters and stellar populations, as well as uncertainties of the dust extinction coefficient[45,52]. SITELLE's spectral information is critical to disentangle the effect of the different parameters (age, mass, Av). It allows for the removal of the contamination from the diffuse ionized gas, the subtraction of the underlying stellar population, as well as the correction for the dust extinction.

Understanding the IMF possible dependence on environmental conditions is still the focus of many studies. Clues about the non-universality of the IMF have been reported from diverse programs. From the difference in the Hα equivalent width measured within integrated spectra in small and large sample of galaxies (Ultra faint dwarfs[47]; NGC 4395 & NGC 5457[24]; 10 000 SDSS galaxies[61]), a break in the HII region luminosity functions[4,9], to the detailed analysis of a few nearby clusters[33], IMF variations are brought forward when observations deviate from the predictable trend. In elliptical galaxies, two main techniques were used to test the IMF stability: 1) the strength of some spectral features sensitive to surface gravity (dwarf, low-mass stars) along with spectral synthesis models and 2) the dynamical determination of the stellar mass with respect to the expected mass-to-light ratio[20,121]. Many studies based on these techniques have claimed that the IMF is not universal. Nevertheless, according to Smith[117], these methods were not reliable as one can conclude that the IMF is universal by neglecting to consider various stellar populations abundances and ages[118] or a different dark matter contribution to the dynamics (e.g. ATLAS3D[27]). A statistical study of IMF variations based on elliptical galaxy stellar content is not an easy task. Although it can provide clues for the non-universality of the IMF, it cannot set constraints on its slopes for different galactic environments. Furthermore, these studies are focused on the lower end of the IMF (the low-mass stars) that will influence the enrichment of the ISM much later in the timescale of a galaxy. In comparison, massive star IMF variations have a greater contribution to the ISM evolution on a shorter timescale. To have a better portrait of the ISM enrichment throughout cosmic time, we need to know if and how the upper end of the IMF changes with respect to environmental conditions. The analysis of a large sample of HII regions and YSCs covering all environments offers a promising angle to answer this question.

Indeed, a vast sample of HII regions with diversified physical properties is a necessary ingredient to derive rigorous constraints to study changes in the IMF as a function of environment. **While HII region parameters are strongly coupled in most spectral analyses (mass, metallicity, dust extinction, IMF, and age), SIGNALS will provide a robust, independent assessment of their separate contributions to the IMF.** Recovering the physical properties of the ionized gas requires observations from many emission lines spread over a wide range in the spectrum[11,97]. Adjacent line ratios have been used to study HII regions and the DIG when no dust correction was applicable (i.e. [NII]λ6548,6583/Hα and [OIII]$\lambda\lambda$4959,5007/Hβ). In order to unlock other line ratios, we include the dust extinction in our model for the spectral analysis. To do so, we will use photoionization models and include the dust correction function[21] within the procedure that extract the parameters of the HII regions. The extinction law of Cardelli et al. [21] will be used and the color excess $E(B-V)$ will be evaluated from the known equation: $E(B-V) =$

$\frac{2.5}{1.07}\log\left((F_{H\alpha/H\beta\,obs})/(F_{H\alpha/H\beta\,theo})\right)$, with $F_{H\alpha/H\beta\,theo}$ given by the photoionization models, and $E(\beta-\alpha)/E(B-V)=1.07$.

Additionally, with a sufficiently large sample of HII regions ($\sim 1\,000$[14,107]), the age and mass distribution is random whereas with a small sample, stochastic sampling of the mass or the age can impact the slope of the luminosity function masking the effect of possible IMF variations. SIGNALS can lift such degeneracies. The robustness of this technique relies largely on the wide range of sampled HII regions, and this is the main reason why SIGNALS' IMF characterization will be more complete than any other studies. The method used to constrain the age and the mass involves stellar population synthesis models. In our case, we will use single stellar population (SSP) models with the appropriate age to represent the young stellar population. The superimposed old stellar population (from the disk and bulge) will be accounted for by considering the absorption spectrum of regions in the galaxy that are adjacent to the HII region studied. The mass of the HII regions is obtained from the factor used to scale the continuum level of the SSP model. The uncertainty on the mass will mainly depend on the signal-to-noise ratio of the spectrum. The mass detection threshold (3σ) in external regions is estimated of the order of $1\,000\,M_\odot$ and its uncertainty (1σ) will range from 500 to $5\,000\,M_\odot$. The precision on the age will vary from 0.5 Myr for very young regions to 10 Myr for older regions. By using three SITELLE's spectral bands (SN1, SN2, and SN3), and additional data in the UV from GALEX (Galaxy Evolution Explorer) and LEGUS, our survey will characterize the age and the mass of YSCs within most of HII regions. The Ultraviolet Imaging Telescope (UVIT) is also providing images at spatial resolution near $1''$ ($30'$ FOV, 120-550 nm). Three team members (Pati, Drissen, and Robert) have privileged access to UVIT data for many of our targets. Constraints on the YSC properties (mass, age, and metallicity) will be fixed by means of combined predictions from 1) the spectro-photometric model, 2) models of HII region ionized structure, 3) comparison of the gas emission with YSC models (i.e. Balmer lines EW[49,80]), and 4) simulations of clouds and YSC populations[101]. Consequently, SFRs will be derived more accurately. Uncertainties on the SFR can originate from underlying old clusters' continuum contamination, and also from the fraction of ionizing photons leaking from the region.

Escaping photons - A better estimate for the escaping photon fraction will have an impact on the accurate determination of the HII region mass-luminosity relation, the HII region ages, and ultimately, the calibration of the SFR indicators[48,126]. By comparing the HII region model predictions and the derived YSC properties, we will estimate the escaping photon fraction. As our sample will cover the whole HII region space of parameters, it will provide strong constraints on the escaping fraction for a broad range of environments. It will also be helpful in recalibrating some extensively used SFR indicators ($SFR_{[OII]}$, $SFR_{[OIII]}$, and $SFR_{H\alpha}$). The fraction of escaping photons is a critical element and may vary from 0%∼80% from region to region. This fraction influences the amount of radiative energy transfered from star-forming regions to the surrounding ISM and the strenght of the DIG (See Sect. B).

A.3 Star Formation Efficiency - Ionized vs Neutral Gas Component

One cannot determine the star formation efficiency (SFE) of an HII region without comparing the mass of the newly formed star cluster and the amount of neutral gas still present in the surroundings. Fortunately, existing molecular and neutral gas maps (CO and HI) of numerous nearby galaxies are now available at a spatial resolution comparable to what SIGNALS will achieve (e.g. ALMA, VLA/IRAM, BIMA, and eventually with NOEMA; see Technical Justification Sect. C and the CSV file for detailed information on the additional data available for each target). All galaxies of the sample but five have been observed with interferometers (VLA, Westerbork, and/or ATCA) at 1.4 GHz (HI). The data quality is homogeneous since ∼60% of the targets have been observed as part of surveys (e.g. [59, 92, 122]). **These neutral hydrogen data will allow us to 1) probe changes in the relative contributions of bursty and quiescent star formation as a function of neutral hydrogen surface density, 2) look for evidence of downsizing by comparing the star formation densities as a function of galaxy mass, 3) identify the drivers of turbulence that sets the velocity dispersions in the neutral hydrogen.** In synergy with SIGNALS, these datasets will provide important information on the resolved star formation efficiency. The amount of gas in the neutral reservoir is an environmental element susceptible to be link to IMF variations. Therefore, SIGNALS will look into the behavior of star formation in dense and gas-poor areas.

B Feedback Processes

B.1 Mass and Energy Returned into the ISM by Stars

Feedback processes that may be affecting the SFE will also be under the scope of SIGNALS. In a star-forming galaxy, the ISM is actively modified and recycled. Massive OB stars in YSCs are not only responsible for ionizing the surrounding gas but also for exercising direct radiative pressure onto this gas, and for returning enriched material and mechanical energy through their stellar winds and supernova explosions. The latter release a sudden burst of energy of the order of 10^{51} erg, causing shock waves propagating through the ISM at several $1\,000\,km\,s^{-1}$, compressing and heating the ISM and changing its metallicity. As an example, Figure 10 shows the local variation of a metallicity indicator observed with SITELLE near a supernova remnant and a young stellar object within NGC 604, a giant HII region in M33. Additionally, models and observations show that the integrated wind mechanical energy from a YSC may be comparable to that of its SN explosion phase[78]. Rotating stars and binaries may also contribute to a longer period of ionizing photon production[35,80,101]. Less massive stars, more numerous, also bring a significant amount of material and ionizing photons into the ISM[104] on a longer time scale and with a poorer metal content compared to massive stars.

With mass-loss rates of 10^{-7}-$10^{-5}\,M_\odot\,yr^{-1}$ and terminal velocities of 1 000 - 3 000 km s^{-1}, massive stars create hot low-density regions bounded by expanding interstellar shells and/or bubbles. For example, a clear link between the Milky Way stellar clusters DBS 160 and 161 and the surrounding HI bubble B332.5-0.1-42 was seen by comparing the stellar wind mechanical energy and gas kinetic energy[28]. Nevertheless the stellar cluster energy conversion efficiency is highly variable between the theory (20%[123]) and observations (2-5%[19]). Shocks from stellar winds have been observed in the X-rays (e.g.[119]). However, to fully account for the observed X-ray luminosity, a non-uniform ISM had to be considered, producing a porous shell from which the hot gas can leak[55]. While the efficiency of stellar winds involved in shaping the HII region bubble is still uncertain, it was also proposed that radiation pressure may play a dominant role at a younger age, while thermal pressure of the warm ionized gas may become more important at a later age[82]. A wide variety of mechanisms have been considered to explain the missing energy from four Milky Way and LMC YSC[105]: radiative cooling, mechanical work on the cold dense shell bounding HII regions, thermal conduction, heating of the dust by collisions with hot gas, and leakage of the hot gas from HII regions (e.g. champaign effect). While this last mechanism may seem sufficient, others produce an amount of energy that is too small compared to the observed wind energy or are too improbable; small-scale mixing of the hot and cold gas leading to turbulent conduction was then suggested to take place.

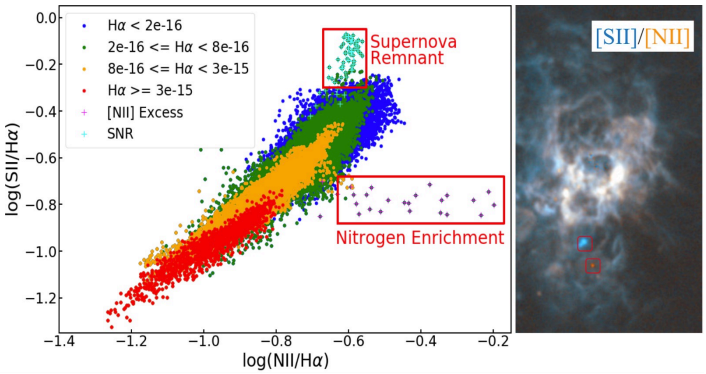

Figure 10: SITELLE's [SII]/[NII] image of the young star forming cluster NGC 604 in M33 and a pixel-by-pixel (0.32″ resolution) BPT diagram. Pixels associated to a supernova remnant and a peculiar [NII] rich object are identified by red squares.

Feedback from massive star clusters is believed to be quenching star formation in a cluster through the removal of its cold gas, resulting in a low SFE[46,76,116]. Still the relation between the ISM and the stellar cluster feedback remains complex as short/truncated star-forming episodes are not always clear. This is supported by individual observations, like in the LMC cluster NGC 602 where star formation seems to be self-propagating to larger cluster radii over 4 Myr[22], and by the migration of starbursts through dwarf galaxies over 500 Myr[87]. **SIGNALS offers the ability to study at high spatial resolution the energy exchange between stellar clusters and the ISM structure and small-scale dynamics, allowing us to establish the energy balance, ionized gas properties, and the star formation morphology and efficiency.**

B.2 Ionizing Photons: HII Regions vs DIG

Only 10% of the total ionized gas in a galaxy is directly associated with HII regions. The origin of the remaining 90%, the diffused ionized gas (or DIG phase), is more enigmatic. Like HII regions, the DIG is almost fully composed of completely ionized hydrogen, with similar temperatures (~10^4 K), lower densities (0.1 cm^{-3}), and slightly lower ionization states. The DIG can be observed near HII region boundaries. Its emission can be detected in all galaxy structures and can globally be seen up to a distance of 2 kpc from a galaxy disk[12,54].

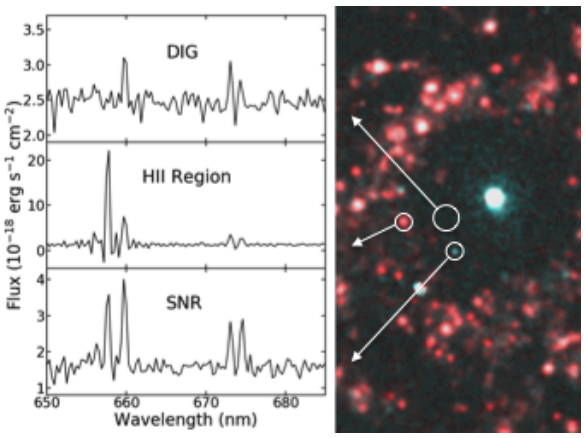

Figure 11: SITELLE's map in the central 1′×2′ region of NGC 3344. Hα (red) and [SII] (blue) are added. The spectrum of 3 different regions is shown. Enhanced DIG emission is found inside the inner ring of this galaxy.

Several sources of ionization might be responsible for the DIG: ionizing photons escaping HII regions and traveling long distances[8,42,53,62,63], a weak AGN[31,57], a generation of post-AGB stars[44], and fast shocks in the ISM (e.g. SNe, galactic structures[2,58]). The DIG was also proposed to be partially related to dust diffusion[114]. Identifying which processes are the most efficient is complex. Our comparison of the DIG signatures in the SITELLE data of the nearly face-on spirals NGC 628 and NGC 3344 (Fig. 11) suggests as well a clear relation with the old stellar population. Larger [SII]/Hα and [NII]/Hα ratios are often used to locate the DIG and the [OII]λ3727 doublet has been proposed to be the main cooling lines of the DIG[39]. In fact, the amount of energy required to keep the DIG ionized is colossal. External heating sources have been ruled out as the DIG intensity has always been linked to the presence of local sources. For that reason, many studies have suggested that only OB stars could be responsible for the DIG emission. However, difficulties remain in explaining how ionizing photons could reach such large distances away from the galaxy plane and disk HII regions. More accurate models of the photon escape fraction for NGC 157[132] have shown that the DIG emission seems to be mostly related to HII region leakage. Detailed numerical simulations predict that the photon escape fraction varies considerably over a few millions years timescale due to the turbulent nature of the gas and can reach up to 37%[62] since the ionizing front can reach lower density medium (depending on the density and porosity of the ISM and the stellar evolution phase of the cluster's massive stars). Also, semi-analytic feedback models for cloud dissolution[101] have demonstrated that the SFE is linked to the ionizing photon escape fraction (high SFE corresponds to a high fraction of escaping photons).

B.3 The DIG Component

A typical spectrum of the DIG observed in the Milky Way has been created[12] with the objective to separate the DIG contribution from the emission of HII regions in nearby galaxies (i.e. to isolate HII region spectra). This technique is relevant in the context of a galaxy with a DIG content similar to the Milky Way. However, from one galaxy to another, and also within one galaxy, the contribution of the DIG can change significantly, and the main heating mechanism could be different, resulting in an atypical DIG spectrum. A study of three galaxies of the Sculptor Group[60] indicates that 30-50% of the Hα line is emitted by the DIG component, and that there is no trend with the morphology or the SFR of the galaxies. It is also established that the line ratios observed in the DIG cannot be explained completely by dust scattered light; only 20% of the DIG is caused by dust scattering[7], against other findings[114]. Instead, the relative DIG emission was linked to the different morphology of the ISM. The state of the gas content (i.e. its density, abundance, temperature, distribution) in galaxies can also modify the ability of the escaping photons to reach large distances and produce the DIG widely spread emission. **The porosity of the ISM (fractal morphology), caused by turbulent convective motion[40], makes the mean free path of ionizing photons much larger than with the standard cloud model[37,38,126,127]. This is a fundamental element in explaining the DIG found far from HII regions. From these observations and findings, it is obvious that the extended DIG emission has a great scientific potential for the study of abundances in galactic halos, and abundance dispersion in disks, as well as for understanding the ISM structure in galaxies. SIGNALS will include the DIG in its analysis in order to have a full view of the ISM properties.** By measuring the relative contribution of the HII regions emission to their surrounding DIG, we will get precise constraints on the fraction of radiation and hot gas escaping the regions and merging with the low density ISM. This information will have a great impact on our understanding of the star formation quenching mechanisms throughout cosmic time once we will have compared different sets of HII region leakage levels and their environmental parameters.

C Small Scale Dynamics

The combined study of gas abundances and kinematics on small scales (≤ 50 pc) as well as large ($\geq$1 kpc) scales holds key information on the chemical evolution of galaxies, notably on the enrichment phases and mixing mechanisms. Theoretical studies exploring mixing mechanisms, their time scales, and how they translate in decreased (or enhanced) abundance fluctuations in the ISM are rather sparse[32,41,71], partly because of a lack of high-spatial resolution studies in large samples of HII regions, as we propose here. A pioneerd paper[109] shows that abundance fluctuations caused by local enrichment can be wiped out by: turbulent diffusion on large scales (1-10 kpc) in the shear flow of differential rotation within a timescale of 1 Gyr; mixing at intermediate scales (100-1 000 pc) due to cloud collisions, super-shell expansion, and differential rotation (0.1 Gyr); and turbulent diffusion, Rayleigh-Taylor and Kelvin-Helmholtz instabilities on small scales ($\leq$100 pc, 2 Myr). Similar arguments related to turbulent mixing were explored recently[93,95]. Other factors, such as inflows, outflows[3,10], as well as dynamical stellar and gas radial migration[50], are believed to alter the chemical composition and its distribution across galaxy disks. Inhomogeneous closed-box models of chemical evolution without mixing[90] suggest that [O/H] dispersion as large as 0.2-0.3 dex could be observed locally in the ISM. In short, the amplitude of abundance fluctuations is related to the local enrichment, but also to the timescale and efficiency of different mixing mechanisms operating on distinctive spatial scales.

On the observational front, the large-scale radial distribution of [O/H] has been established in hundreds of galaxies[110,111,130]. However, studies of azimuthal variations have been more limited, mostly due to large uncertainties often affecting individual [O/H] values or small HII region sample sizes[15,25,29,36,67,81,84,103,112]. Moreover, multiple studies have investigated the global HII region dynamical properties from the turbulent motion of the gas, to the expansion velocity of the HII regions shell[9,13,14,18,23,64,99,128,129,131]: it was found that the velocity dispersion within an HII region scales with its luminosity and additionally, some observed a break in the luminosity function, a result consistent with a transition between the core collapse and competitive accretion regimes of star formation. Despite these significant advances, a systematic study of the nebular gas abundance fluctuations and dynamics to assess the impact of stellar winds, supernova explosions and other sources on the mixing processes and the star formation activity has not been done yet on the scale and with the physical spatial resolution proposed by SIGNALS.

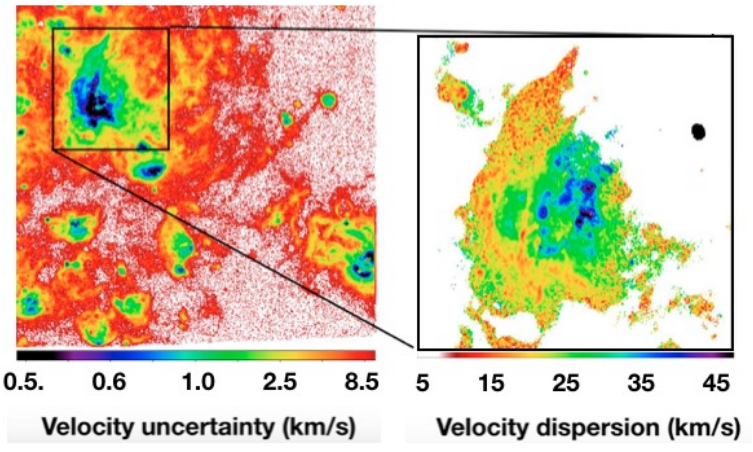

Figure 12: M 33 Hα velocity uncertainties and dispersion for a small portion of the SITELLE FOV with R = 3 000.

The spectral resolution provided by SITELLE SN3 cubes for five lines simultaneously (R = 5 000 for the Hα, [NII]$\lambda\lambda$ 6548,6583, and [SII]$\lambda\lambda$6717,6731 emission lines), combined with deconvolution capabilities using a Bayesian approach (using ORCS; see Technical Justification Sect. F.2), will allow us to determine the line centroid with a precision of 0.2 to 10 km/s across the FOV, to detect line broadening larger than 10 km/s in most HII regions (see Fig. 12), and

separate multiple components along the line of sight[86]. Combined with the line ratio analysis discussed in previous sections, several aspects of the ionized gas dynamics on all scales (from barely resolved objects such as supernova remnants, to HII regions and large-scale features), will be probed: 1) turbulent motions and shell expansion velocity in HII regions, from which their mass can be determined; 2) kinematics and abundance patterns linked to the different mixing mechanisms and abundance variations; 3) rotation curves, and gas pressure support (or gas asymmetric drift) to derive more accurate circular velocity curves and mass distribution models of the galaxies[30,98]; 4) residual velocity maps, and high-order harmonics fit of the velocity and velocity dispersion maps, to investigate the perturbations due to spiral arms and bars, gas migration[112], gas driven inwards radially to fuel Starburst galaxies or AGN; 5) structure of orbits of ionized gas in the disk plane, as measured from the azimuthal anisotropy parameter of the gas random motions; 6) the kinematics of the ionized gas compared with the neutral gas and/or stellar kinematics[79].

D Local Environment Influence and Stellar Populations

The SIGNALS project will focus on studying the star formation process as a whole. To investigate possible relations between star-forming regions and their environment, the following parameters will be taken into account: the local stellar density, local DIG background, local neutral gas density, local SFR and SFE, and distances to the nearest region and to prominent galactic structures (bar, spiral arm, and AGN). **The size, global geometry, and total Hα luminosity of each region, extracted from a profile fit of the Hα map, are also important. Defining these values for each of the 50 000 regions allows us to conveniently categorize regions using these criteria. The luminosity functions for low and high DIG background (as shown in Figure 4) are one example of the possible trends that can be extracted using all this combined information.** In this particular case, HII regions with a high DIG background were in general more massive and located within high SFR zones along the galaxy spiral arms. Another example is the link between the size of a region and its luminosity. Figure 13 shows the integrated Hα luminosity as a function of the mean radius of the emission line region. The color scale is related to the correlation coefficient of the profile fit (on the left) and to the DIG background level measured (on the right). On the same figure, models allow us to verify how well a region can be depicted by a Strömgren sphere.

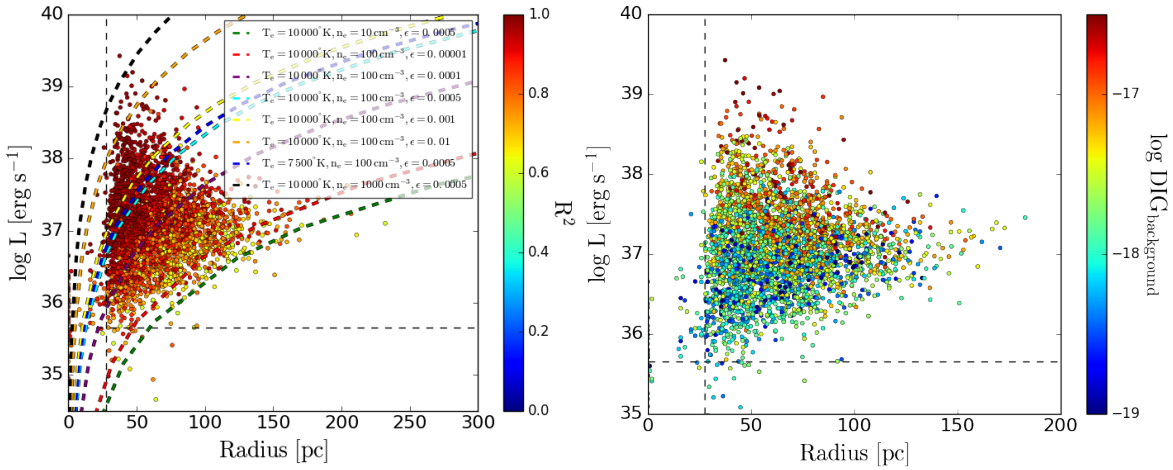

Figure 13: NGC 628 HII region candidates integrated Hα luminosity as a function of their radius obtained when comparing them with Strömgren sphere models[107]. Only regions with a correlation coefficient R^2>0.6 are shown. On the left, the dashed curves represent the luminosity and radius relation for theoretical Strömgren spheres considering various stellar cluster masses, electron temperatures T_e and densities n_e, and volume filling factors ϵ, as indicated in the plot. For each dashed curve, the cluster mass increases from the left to the right. The vertical dashed line is the sensitivity threshold of the Hα intensity distribution for the Strömgren model extracted from the relation between the σ of the Gaussian for the intensity profile and Strömgren radius R_S (overplotted in the left lower corner); The horizontal dashed line is the luminosity detection limit. On the right, same plot with a color scale representing the level of the DIG background ($\log \mathrm{DIG}_{background}$ in erg s^{-1} cm^{-2}) measured in the surroundings of each region.

D.1 Stellar Populations and Individual Stars

A large variety of galaxies with different stellar populations and stellar densities can be found within the SIGNALS sample. Within each individual target this distribution also changes dramatically from one area to another. The analysis method used to extract the spectral information must be adapted to various situations. At the same time, uniformity in the analysis must be preserved across the survey. In addition, as the spatial resolution goes from ∼2 to 40 pc, the analysis of the stellar continuum goes from performing aperture photometry on individual stars to extracting integrated spectra of resolved stellar clusters mixed with the surrounding stellar populations. Although the diversity of targets adds complexity to the analysis, it is a strength for SIGNALS since reliable size subsamples can be used for specific purposes in addressing the main goals of the project. The nearest galaxies enable resolving individual stars and test stochastic sampling effects for the massive star IMF on the HII region emission and derived parameters. On the other hand, more distant galaxies increase the number of regions in one FOV, useful to study of global variations of the massive star IMF and their impact on the derived SFR with statistically reliable sample of HII regions within different environments.

For most galaxies, the analysis method used to account for the presence of the stellar continuum includes selecting apertures for sampling the SED and stellar absorption components to build a reference spectrum. The shape of the

reference spectrum extracted depends on the instrumental line profile (sinc) as well as on the instrument configuration during observations (sampling of the interferograms). Therefore, extracting it directly from the data has the advantage of accounting for all of these factors. The continuum level in the different filters is used to approximate the stellar density in the surroundings of the HII regions.

E SIGNALS Legacy Value

SIGNALS is unique. This legacy survey will provide new, key insights on star formation, chemical enrichment, and feedback mechanisms driving the evolution of the ISM and galaxies. The high sensitivity and good spatial resolution of SITELLE will allow us to explore statistically significant samples of HII regions (∼50 000 regions) with different characteristics and stellar populations, in various environments. From multiple nebular lines, physical properties like abundances, ionization structure, and dynamics will be obtained for these regions as well as information on the DIG and the IMF variability. SIGNALS will pave the way to understanding more distant galaxies with a better interpretation of their SFR indicators at a lower spatial resolution. SIGNALS dataset will be extremely rich and valuable for investigating many other physical mechanisms as well. **To cite only a few complementary and important research topics that can be studied: 1) planetary nebula abundance distributions and luminosity functions[75,85]; 2) supernova remnant ionization conditions, occurrence, and feedback contribution; 3) detection of background emission line objects (e.g. [OII] and Ly-α emitters); and 4) large-scale velocity mapping of galaxies to build mass models. A total of 325 hours (50 nights) of telescope time is requested over eight semesters.** Our ideal sample of targets includes more objects than required to fill the 50 nights requested. Therefore, depending on the telescope pressure during each semester, the target sample can be adapted to match the available windows and facilitate scheduling. More details about the sample can be found in the Technical Justification.

References:

[**1**] A. Adamo et al. ApJ 841, 131 (2017). [**2**] M. G. Allen et al. ApJS 178, 20 (2008). [**3**] B. H. Andrews et al. ApJ 835, 224 (2017). [**4**] J. E. Andrews et al. ApJ 767, 51 (2013). [**5**] M. Azimlu, R. Marciniak, and P. Barmby. AJ 142, 139 (2011). [**6**] J. A. Baldwin, M. M. Phillips, and R. Terlevich. PASP 93, 5 (1981). [**7**] J. E. Barnes et al. MNRAS 447, 559 (2015). [**8**] J. E. Barnes et al. MNRAS 440, 3027 (2014). [**9**] J. E. Beckman et al. AJ 119, 2728 (2000). [**10**] D. A. Berg et al. ApJ 806, 16 (2015). [**11**] G. A. Blanc et al. ApJ 798, 99 (2015). [**12**] G. A. Blanc et al. ApJ 704, 842 (2009). [**13**] J. Blasco-Herrera et al. MNRAS 407, 2519 (2010). [**14**] T. R. Bradley et al. A&A 459, L13 (2006). [**15**] F. Bresolin. ApJ 730, 129 (2011). [**16**] D. Brousseau et al. Vol. 9147. Proc. SPIE. 2014, 91473Z. [**17**] J. J. Bryant and J. Bland-Hawthorn. Vol. 8446. Proc. SPIE. 2012, 84466K. [**18**] H. E. Caicedo-Ortiz et al. Vol. 582. Journal of Physics Conference Series. 2015, p. 012049. [**19**] C. E. Cappa et al. Ed. by K. van der Hucht, A. Herrero, and C. Esteban. Vol. 212. IAU Symposium. 2003, p. 596. [**20**] M. Cappellari et al. Nature 484, 485 (2012). [**21**] J. A. Cardelli, G. C. Clayton, and J. S. Mathis. ApJ 345, 245 (1989). [**22**] L. R. Carlson et al. ApJ 665, L109 (2007). [**23**] H. O. Castañeda and M. Rozas. Ed. by W. J. Henney, J. Franco, and M. Martos. Vol. 12. RMxAA. 2002, p. 236. [**24**] B. Cedrés, J. Cepa, and A. Tomita. ApJ 634, 1043 (2005). [**25**] B. Cedrés et al. A&A 545, A43 (2012). [**26**] G. Chabrier. PASP 115, 763 (2003). [**27**] B. Clauwens, J. Schaye, and M. Franx. MNRAS 449, 4091 (2015). [**28**] M. A. Corti et al. A&A 588, A63 (2016). [**29**] K. V. Croxall et al. ApJ 830, 4 (2016). [**30**] J. J. Dalcanton and A. M. Stilp. ApJ 721, 547 (2010). [**31**] R. L. Davies et al. MNRAS 439, 3835 (2014). [**32**] M. A. de Avillez and M.-M. Mac Low. ApJ 581 (2002). [**33**] S. Dib. MNRAS 444, 1957 (2014). [**34**] M. A. Dopita and R. S. Sutherland. ApJ 455, 468 (1995). [**35**] J. J. Eldridge and E. R. Stanway. MNRAS 400 (2009). [**36**] S. L. Ellison et al. MNRAS 416, 2182 (2011). [**37**] B. G. Elmegreen. PASA 15, 74 (1998). [**38**] B. G. Elmegreen et al. ApJ 644 (2006). [**39**] T. Elwert and R.-J. Dettmar. Ed. by R. Braun. Vol. 331. ASP. 2005, p. 203. [**40**] D. Falceta-Gonçalves et al. MNRAS 446, 973 (2015). [**41**] Y. Feng and M. R. Krumholz. Nature 513 (2014). [**42**] A. M. N. Ferguson et al. AJ 111, 2265 (1996). [**43**] G. J. Ferland et al. PASP 110, 761 (1998). [**44**] N. Flores-Fajardo et al. MNRAS 415, 2182 (2011). [**45**] M. L. García-Vargas, M. Mollá, and M. L. Martín-Manjón. MNRAS 432, 2746 (2013). [**46**] E. Gavagnin et al. MNRAS 472, 4155 (2017). [**47**] M. Geha et al. ApJ 771, 29 (2013). [**48**] J. M. Gomes et al. A&A 586, A22 (2016). [**49**] R. M. González Delgado et al. MNRAS 357, 945 (2005). [**50**] R. J. J. Grand, D. Kawata, and M. Cropper. MNRAS 447, 4018 (2015). [**51**] K. Grasha et al. ApJ 815, 93 (2015). [**52**] A. S. Gusev et al. MNRAS 457, 3344 (2016). [**53**] L. M. Haffner et al. *RMP* 81, 969 (2009). [**54**] L. M. Haffner, R. J. Reynolds, and S. L. Tufte. ApJ 523, 223 (1999). [**55**] E. Harper-Clark and N. Murray. ApJ 693, 1696 (2009). [**56**] I.-T. Ho et al. MNRAS 444, 3894 (2014). [**57**] L. C. Ho. ARA&A 46, 475 (2008). [**58**] T. L. Hoffmann et al. A&A 544, A57 (2012). [**59**] B. W. Holwerda, N. Pirzkal, and J. S. Heiner. MNRAS 427 (2012). [**60**] C. G. Hoopes and R. A. M. Walterbos. ApJ 586, 902 (2003). [**61**] E. A. Hoversten and K. Glazebrook. ApJ 675, 163 (2008). [**62**] C. Howard, R. Pudritz, and R. Klessen. ApJ 834, 40 (2017). [**63**] C. S. Howard, R. E. Pudritz, and W. E. Harris. MNRAS 461 (2016). [**64**] J. Jimenez-Vicente et al. Ap&SS 276, 445 (2001). [**65**] G. Kauffmann et al. MNRAS 346, 1055 (2003). [**66**] R. C. Kennicutt Jr. ARA&A 36, 189 (1998). [**67**] R. C. Kennicutt Jr. and D. R. Garnett. ApJ 456, 504 (1996). [**68**] L. J. Kewley and S. L. Ellison. ApJ 681, 1183 (2008). [**69**] L. J. Kewley et al. ApJ 556, 121 (2001). [**70**] L. J. Kewley and M. A. Dopita. ApJS 142, 35 (2002). [**71**] R. Klessen and D. Lin. *Astronomische Nachrichten Supplement* 324 (2003). [**72**] A. Y. Kniazev et al. AJ 130, 1558 (2005). [**73**] J. A. Kollmeier et al. *ArXiv e-prints* (2017). [**74**] I. Konstantopoulos et al. Vol. 221. AAS. 2013, p. 215.01. [**75**] K. Kreckel et al. ApJ 834, 174 (2017). [**76**] M. R. Krumholz et al. *Protostars and Planets VI*, 243 (2014). [**77**] F. Laurent et al. PASP 118, 1564 (2006). [**78**] C. Leitherer, C. Robert, and L. Drissen. ApJ 401, 596 (1992). [**79**] G. Y. C. Leung et al. MNRAS (2018). [**80**] E. M. Levesque and C. Leitherer. ApJ 779, 170 (2013). [**81**] Y. Li, F. Bresolin, and R. C. Kennicutt Jr. ApJ 766, 17 (2013). [**82**] L. A. Lopez et al. ApJ 795, 121 (2014). [**83**] J. López-Hernández et al. MNRAS 430, 472 (2013). [**84**] P. Martin and J. Belley. ApJ 468, 598 (1996). [**85**] T. B. Martin, L. Drissen, and A.-L. Melchior. MNRAS 473 (2018). [**86**] T. B. Martin, S. Prunet, and L. Drissen. MNRAS 463, 4223 (2016). [**87**] K. B. W. McQuinn et al. ApJ 724, 49 (2010). [**88**] C. Morisset, G. Delgado-Inglada, and N. Flores-Fajardo. RMxAA 51, 103 (2015). [**89**] J. Moustakas, R. C. Kennicutt Jr., and C. A. Tremonti. ApJ 642, 775 (2006). [**90**] M. S. Oey. ApJ 542, L25 (2000). [**91**] D. E. Osterbrock and G. J. Ferland. 2006. [**92**] J. Ott et al. AJ 144, 123 (2012). [**93**] L. Pan. PhD thesis. The University of Texas at Austin, 2008. [**94**] E. Pérez-Montero et al. A&A 566, A12 (2014). [**95**] A. C. Petit et al. MNRAS 449, 2588 (2015). [**96**] L. S. Pilyugin, T. Contini, and J. M. Vílchez. A&A 423, 427 (2004). [**97**] L. S. Pilyugin and E. K. Grebel. MNRAS 457 (2016). [**98**] J. C. B. Pineda et al. MNRAS 466, 63 (2017). [**99**] H. Plana, J. Maíz-Apellániz, and E. Telles. Ap&SS 289, 287 (2004). [**100**] D. Rahner et al. MNRAS 473 (2018). [**101**] D. Rahner et al. MNRAS 470 (2017). [**102**] S. N. Richards et al. MNRAS 455, 2826 (2016). [**103**] F. F. Rosales-Ortega et al. MNRAS 415, 2439 (2011). [**104**] W. K. Rose and D. G. Wentzel. ApJ 181, 115 (1973). [**105**] A. L. Rosen et al. MNRAS 442, 2701 (2014). [**106**] M. M. Roth et al. PASP 117, 620 (2005). [**107**] L. Rousseau-Nepton et al. MNRAS (2018). [**108**] Laurie Rousseau-Nepton. PhD thesis. Université Laval, Québec, 2017. [**109**] J.-R. Roy and D. Kunth. A&A 294, 432 (1995). [**110**] S. F. Sánchez et al. A&A 563, A49 (2014). [**111**] S. F. Sánchez and L. Sánchez-Menguiano. Vol. 49. RMxAA. 2017, p. 28. [**112**] L. Sánchez-Menguiano et al. ApJ 830, L40 (2016). [**113**] F. R. N. Schneider et al. *Science* 359, 69 (2018). [**114**] K.-I. Seon and A. N. Witt. ApJ 758, 109 (2012). [**115**] S. Sharma et al. A&A 534, A96 (2011). [**116**] K. Shima et al. PASJ (2017). [**117**] R. J. Smith. MNRAS 443, L69 (2014). [**118**] C. Spiniello, S. C. Trager, and L. V. E. Koopmans. ApJ 803, 87 (2015). [**119**] L. K. Townsley et al. ApJS 194, 1 (2011). [**120**] N. Vale Asari et al. MNRAS 460, 1739 (2016). [**121**] P. G. van Dokkum and C. Conroy. Nature 468, 940 (2010). [**122**] F. Walter et al. AJ 136, 2563-2647 (2008). [**123**] R. Weaver et al. ApJ 218, 377 (1977). [**124**] J. A. Weber, A. W. A. Pauldrach, and T. L. Hoffmann. A&A 583, A63 (2015). [**125**] B. C. Whitmore et al. AJ 147, 78 (2014). [**126**] K. Wood et al. ApJ 633, 295 (2005). [**127**] K. Wood et al. ApJ 770, 152 (2013). [**128**] J. Zaragoza-Cardiel et al. MNRAS 451, 1307 (2015). [**129**] J. Zaragoza-Cardiel et al. MNRAS 432, 998 (2013). [**130**] I. A. Zinchenko et al. MNRAS 462, 2715 (2016). [**131**] A. Zurita et al. A&A 413, 73 (2004). [**132**] A. Zurita et al. A&A 386, 801 (2002).

Technical Justification

The design of SITELLE was optimized for the study of emission-line objects. Studying star-forming regions in nearby galaxies is therefore a natural application for this instrument. A lot of technical challenges were overcome while building the instrument to assure an excellent sensitivity, a high spectral resolution, and a large FOV.

The whole SIGNALS observing strategy is built upon SITELLE's strengths. Three filters are to be used to optimize the detection and characterization of the strong diagnostic lines for nearby extragalactic nebulae: SN1 (363-386 nm) with the [OII]λ3727 and the Balmer emission lines H9 to H12 (detected in bright regions), SN2 (482-513 nm) with Hβ and [OIII]$\lambda\lambda$4959+5007, and SN3 (647-685 nm) with Hα, [NII]$\lambda\lambda$6548+6583, HeIλ6678, and [SII]$\lambda\lambda$6717+6731. These filters are wide enough to provide an excellent sampling of the continuum on each side of the emission lines. They also enable the study of the absorption lines from the stellar populations (Balmer lines and, e.g., Fe+Caλ6490) in galaxy disks and young star-forming regions to properly correct the emission lines.

Need for dark/grey time - A well-known disadvantage of an IFTS over a dispersive spectrograph is the distributed noise: the spectral range covered by the filter is not scanned wavelength by wavelength - photons from the entire bandpass are collected at each mirror step contributing to the noise at each wavelength. Although the data product is a collection of 4 million spectra, SITELLE must be considered as an imager for the Moon phase contribution to the noise. Therefore, observations with SN1 and SN2 require dark time while observations with SN3 can tolerate some moonlight (see simulations included below).

Spectral calibration - The spectral calibration is obtained with a He-Ne laser datacube, combined with a detailed analysis of the phase map of the datacube itself. In our case, the best spectral calibration is required for the SN3 filter for kinematic studies. Numerous night-sky OH lines are found on each end of the SN3 waveband allowing a sub-km/s precision for the absolute radial velocity of the gaseous components.

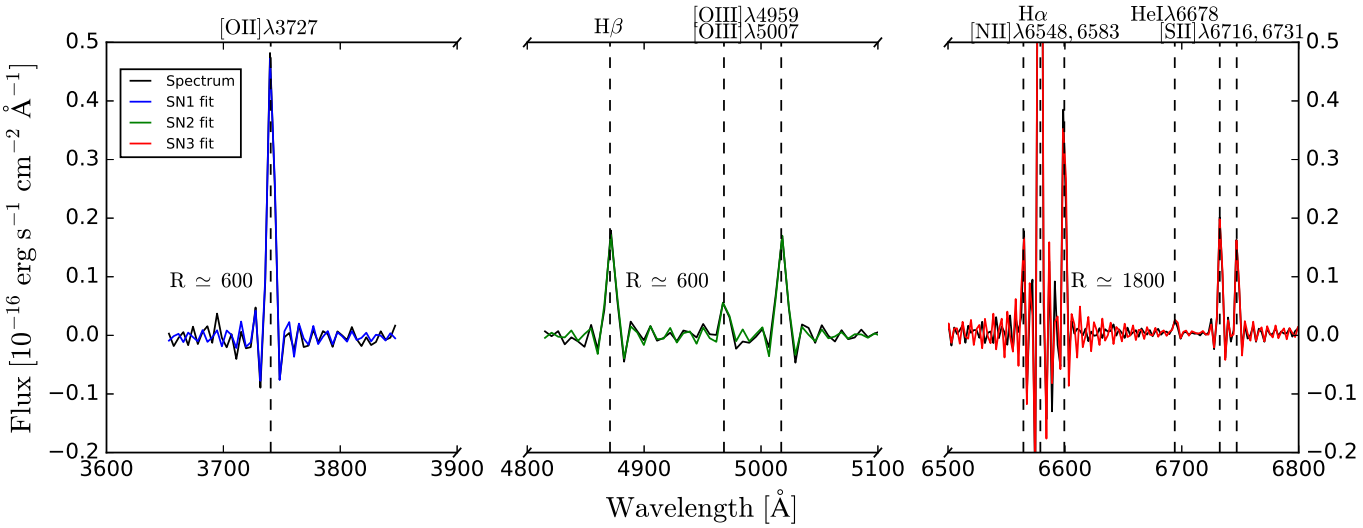

Figure 14: Continuum subtracted spectrum of an HII region in NGC 628 extracted from the datacubes using a circular aperture with a radius of 1.6″, centered at RA 01h36m53.1s and DEC +15°48′04.8″. The fits obtained with ORCS (see Sect. F.2) for the emission lines (§ 3) are shown. Note that SITELLE's line profiles are fitted using a sine cardinal function.

A Instrument Configuration

Calibrations – Flux (i.e. flats images and standard star images) and wavelength calibration (i.e. He-Ne datacube) are required. Seeing - A limit of 1.2″ is selected to set the spatial sampling of the HII regions.

Filter configurations - Essential nebular lines ratios are compiled in Tab. 1. The SITELLE Exposure Time Calculator (ETC) was used to simulate the expected signal-to-noise ratio on specific lines and fix the instrumental configurations (i.e. resolution, exposure time, and Moon maximal contribution) for SN1, SN2, and SN3. Figure 14 shows an example of an HII region spectrum produced with SITELLE with these three filters.

Table 1: Line ratios used in SIGNALS

Ratio	Definition
R2	[OII]λ3727/Hβ
O3O2	[OIII]$\lambda\lambda$4959+5007/[OII]λ3727
R23	([OII]λ3727+[OIII]$\lambda\lambda$4959+5007)/Hβ
R3	[OIII]$\lambda\lambda$4959+5007/Hβ
O2N2	[OII]λ3727/[NII]$\lambda\lambda$6548+6583
N2	[NII]$\lambda\lambda$6548+6583/Hα
S2	[SII]$\lambda\lambda$6717+6731/Hα
N2S2	[NII]$\lambda\lambda$6548+6583/[SII]$\lambda\lambda$6717+6731
O3N2	[OIII]$\lambda\lambda$4959+5007/[NII]$\lambda\lambda$6548+6583

SN3 filter (6480 - 6850 Å) - The SN3 spectral band will allow us to study the ionized gas dynamics, the SFR, the IMF, etc. It also contains key lines used for important line ratios (e.g. N2, S2, N2S2, O3N2, Hα/Hβ) required for our analysis of the HII regions and the DIG. HII region Hα surface brightness (SB) ranges from $\sim 8\times10^{-17}$ to 8×10^{-12} erg s^{-1}cm^{-2}arcsec^{-2}. Using a mean spatial sampling of 0.96″ (3 pixels), we estimate that the faintest regions would be detected with a total exposure time of 14 398s. With the SN3 configuration (R = 5 000, I time = 14 398 s [3.8 s overheads], exptime = 13.3 s step^{-1}, 842 steps), the detection threshold (SNR = 3) will be SB$_{H\alpha} \sim 3.6\times10^{-17}$ erg s^{-1}cm^{-2}arcsec^{-2} (ETC simulation 1). Furthermore, this threshold is ideal for

the detection of the faint DIG component (SB_{DIG}~5×10^{-18} erg s^{-1}cm^{-2}arcsec^{-2}) (using an appropriate binning of the data). Another ETC simulation shows that a moderate contribution of the Moon will not compromise dramatically the HII region detection (SNR = 2.5, ETC simulation 2). With R = 5 000, a precision on the velocity measurements of ~0.1 to 5 km s^{-1} will be reached on most regions[85].

SN2 filter (4840 - 5120 Å) - This filter is used to get the Hβ and [OIII]$\lambda\lambda$4959,5007 lines as well as the crucial dust correction factor E(B-V) from the Hα/Hβ ratio. Once dust corrected, some key ratios of widely separated lines (i.e. N2O2, R2, R23) and the [OII]λ3727 line can be used (an important line for the DIG emission and the photo-ionization modeling). The configuration (R = 1 000, I time = 10 797 s [3.8 s overheads], exptime = 45.5 s step^{-1}, 219 steps) is selected to separate the emission, and to measure the continuum level. The detection threshold on Hβ will be 4.2×10^{-17} erg s^{-1}cm^{-2}arcsec^{-2} for a 0.96″ sampling, corresponding to a $SB_{H\alpha}$ of 1.27×10^{-16} erg s^{-1}cm^{-2}arcsec^{-2} (ETC simulation 3). ETC simulations also show that the Moon can compromise the Hβ detection (New Moon: SNR = 3.0, Crescent Moon: SNR = 2.1, ETC simulations 3 and 4). We estimated that over 30% of the pixels with detection on Hα will have a Hβ detection before applying any spatial binning. After spatial binning, this detection threshold ensures that most HII regions integrated spectra will have a reliable measurement of the Hα/Hβ ratio (>95%; considering a mean extinction of E(B−V)≃0.5).

SN1 filter (3630 - 3850 Å) - The SN1 filter enables the use of important indicators of the gas properties (R2, R23, O32, O2N2). Furthermore, the main line of this filter, [OII]λ3727, is a key diagnostic tool for nebular abundances, the DIG, and the SFR. Its detection depends on several parameters such as the SB, dust extinction, and metallicity. The SN1 configuration (R = 1 000, I time = 10 802 s [3.8 sec overheads], exptime = 59.0 s step^{-1}, 172 steps) is selected to fix the detection threshold for [OII]λ3727 at 3.0×10^{-17} erg s^{-1}cm^{-2}arcsec^{-2} for a 0.96″ sampling, corresponding to a $SB_{H\alpha}$ of 4.0×10^{-18} erg s^{-1}cm^{-2}arcsec^{-2} at solar metallicity (ETC simulation 5). A ETC simulation shows that the Moon can compromise the detection (New Moon: SNR = 3.0, Crescent moon: SNR = 1.5, ETC simulations 5 and 6).

Note about the spectral resolution - The SN1 and SN2 configurations selected represent a good compromise between the total integration time and the amount of pixels available for the high-resolution abundance analysis. The SN1 and SN2 resolution (R = 1 000) is also high enough to compare stellar spectra with models and carries on an additional legacy value for the study of galaxy stellar populations.

In summary, a total of 10.0 hours is required for each of the fields (33 fields in 50 nights).

B Sample Size Justification

As stated several times in this proposal, we want to sample different star-forming environments and to observe enough HII regions in each of them in the interest of properly sampling the luminosity function and overcoming the effect of the stochastic sampling of the regions' age and mass. Table 2 illustrates the main sampling criteria that led to the targets selected and the observing time requested. For each metallicity range studied, we want to subdivide the regions in two to three groups of stellar density, two groups of SFE, and two groups of isolation level (i.e. density of HII regions or distance to the nearest neighbor HII region). If we add together all the regions required (column 5 of Tab. 2), we reach a total of ~56 000 regions. This value matches with the expected number of regions expected in SIGNALS.

Table 2: SIGNALS Environments Sampling

Metallicity range 12+log[O/H]	Stellar density range mag arcsec^{-2}	SFE range $M_\odot$ yr^{-1}	Isolation level	~Regions required*	Where these regions are likely to be found in the sample of galaxies selected
7.5 − 8.0	μ_V<22 $\mu_V\geq$22	<8×10^{-10} ≥8×10^{-10}	<200 pc ≥200 pc	8 000	Regions in dwarf galaxies T8-T9 External regions of T2 to T7
8.0 − 8.25	μ_V<21 $\mu_V\geq$21	<8×10^{-10} ≥8×10^{-10}	<200 pc ≥200 pc	8 000	Regions in dwarf galaxies T8-T9 External regions of T2 to T7
8.25 − 8.5	μ_V<21 21<$\mu_V\geq$20 $\mu_V\geq$20	<8×10^{-10} ≥8×10^{-10}	<200 pc ≥200 pc	12 000	Disk regions of T2 to T7 Central regions of T5 to T8
8.5 − 8.75	μ_V<20 20<$\mu_V\geq$19 $\mu_V\geq$19	<8×10^{-10} ≥8×10^{-10}	<200 pc ≥200 pc	12 000	Disk regions of T2 to T7 Central regions of T4 to T7
8.75 − 9.0	μ_V< 19 $\mu_V\geq$ 19	<8×10^{-10} ≥8×10^{-10}	<200 pc ≥200 pc	8 000	Disk regions of T2 to T4 Central regions of T2 to T4
9.0 − 9.5	μ_V< 19 $\mu_V\geq$ 19	<8×10^{-10} ≥8×10^{-10}	<200 pc ≥200 pc	8 000	Central regions of T2 to T4

* 1 000 regions per bin (ex: 1 metallicity bin × 2 stellar mass bin × 2 SFE bins × 2 Isolation range × 1 000 = 8 000 regions)

To insure that the distribution of the regions covered is representative of our science requirements, we will focus on different types of galaxies and record the completion of each subsample defined here using these parameters : metallicity, stellar density, SFE, and isolation level. The thresholds between the groups of regions for the metallicity range, the stellar density range, the SFE range, and the isolation level might change depending on the natural distribution of the HII regions observed. Some galaxies contain a few hundreds HII regions (e.g. T-8 to T-9) whereas some have more than 4 000 (e.g. T-2 to T-4). Every galaxy type is valuable to SIGNALS since all the different environments must be covered (see column 6 of Tab. 2 and Sect. C of the Technical Justification). For all the reasons mentioned above, SIGNALS could not complete its science goals if the allocated time is significantly reduced.

C Galaxy Sample

The selection of the galaxy sample was driven by the need to observe a very large number of extragalactic HII regions. Star-forming galaxies are therefore our prime selection criteria (these are selected based on the existing Hα and UV-GALEX images), along with a low inclination (i<60^o) to avoid extreme dust extinction. For an unbiased purpose, the target selection is also based on a volume-limited sample. For technical reasons (e.g. to allow a minimum contiguous observing period of 2h), objects with a declination below -22^o and over $+62^o$ are rejected. Using these constraints, a maximum distance of 10 Mpc, and a minimum size of $2'\times2'$ (to maximize the use of the FOV and the number of HII regions), we included 39 galaxies in the sample (plus 13 secondary targets for which we have either relaxed some of the selection criteria for particular reasons or because of their mild level of star-forming activities). Our sample of galaxies covers a wide range of environments: abundances (12+log(O/H) from 7.5 in Sextans A[72] to >9.0 in objects like M51 and M63[96]), in stellar mass (proportional to μ_V) from μ_V below 30 mag arcsec^{-2} up to 18 mag arcsec^{-2}, contents in molecular and neutral gas, and it represents a large variety of galactic structures (size of the bulge, spiral arms, bars, rings, faint external structures, etc.; see Fig. 19).

With our current observing strategy and analysis method, a quick estimate confirms that about 50 000 HII regions will be included in SIGNALS (by extrapolation from the Hα images of the galaxies, the number of fields observed, and the known accuracy of the region identification as a function of spatial sampling).

M33 has already been partially observed and a mosaic of the first four fields has been shown in Figure 1. Additional fields are proposed for both M31 and M33 because of their small distance. Similarly, five other SIGNALS primary targets are close enough to get a spatial resolution below 3 pc. Reaching such a resolution is essential for some objectives of the project aiming at resolving the gas ionization structure and the ionizing star content of the nebulae (e.g. faint end of the HII region luminosity function, calibration of the models with resolved structure of the ionized gas, etc.). The sequence of objects included is fairly well distributed in number and morphological type (see Fig. 17), which is essential for sampling different metallicities and environments. With target distances up to 10 Mpc, we will probe the effect of the spatial resolution on the interpretation of the ionized gas and stellar populations parameters. This is a fundamental step to improve our understanding of the content of more distant galaxies.

The volume-limited sample at 10 Mpc gives a spatial resolution between 2 and 40 pc. Therefore SIGNALS has a spatial resolution advantage to study of the star-forming regions upon other surveys with a typical resolution from 100 pc to >1 kpc (e.g. CALIFA, SAMI, and MANGA). Table 3 shows the comparison between SIGNALS and other IFU surveys of galaxies (and HST LEGUS survey for comparison). SIGNALS objectives are very different, but they are also complementary to those of other surveys. Also, SIGNALS will be ideally complementing the MUSE survey over the northern sky. We meticulously compiled existing data on these galaxies with HST+LEGUS (28 galaxies), GALEX (UV, 39 galaxies), Spitzer (IR, 43 galaxies), BIMA and ALMA (CO, 23 galaxies), VLA (HI, 42 galaxies), as well as narrow bands. These are to be used for future comparisons and to plan other proposals (for example with UVIT and ALMA). The RA target distribution is widely spread (see the Management Plan section and Fig. 19) and the final sample can be adjusted according to the telescope pressure in RA and other instrument scheduling constraints.

Table 3: Comparison of SIGNALS with Other Surveys

SURVEYS	SIGNALS	MUSE	CALIFA	SAMI	MANGA	LEGUS
Instrument	SITELLE	MUSE	PPAK	SAMI	SDSS	HST
Telescope	3.6 m	8.2 m	3.5 m	3.9 m	2.5 m	2.4 m (space)
Total FOV # IFUs IFUs FOV	$11'\times11'$ 1 $11'\times11'$	$60''\times60''$ 1 $60''\times60''$	$74''\times64''$ 1 $74''\times64''$	$1^o\times1^o$ 13 $\sim15''$	$7^o\times7^o$ 17 $12''$ to $32''$	$123''\times136''$ 0 N/A
# Spectra /pointing	4 000 000	90 000	382	793	1423	N/A
Spectral Range	SN1: 363-385 SN2: 484-512 SN3: 648-685 nm	465-930 nm	370-500 nm 430-700	370-580 nm 630-740nm	360-1 000 nm	WFC3: F(275, 336, 438, 555, 814)W ACS: F(435, 814, 606)W
Spectral Resolution	R $\sim$ 5000 at Hα	R $\sim$ 3000	R $\sim$ 850 R $\sim$ 1650	R $\sim$ 1750 R $\sim$ 4500	R $\sim$ 2000	R = 1 Imager
Size (fiber) Filling	$0.32''$ 100%	$0.2''$ 100%	$2.7''$ 65%	$1.6''$ 75%	$2.0''$ 54%	$0.04''$ 100%
Seeing	$\sim0.8''$	0.3-0.4$''$	$<2.7''$	$\sim2.1''$	$<2.0''$	–
# Galaxies	38 (50 000 regions)	20	$\sim$600	3 400	10 000	50 (>> YSC)
z	<0.0037	>0.0025	0.005-0.03	0.004-0.095	$\sim$0.03	<0.0028
Sampling	2-40 pc	$\sim$100 pc	$\sim$1 kpc	1.0-3.3 kpc	1.0-2.0 kpc	$\sim$10 pc
Galaxies common to SIGNALS	–	4	1 NGC628	0	0	12
Main topics	- HII regions properties - ISM properties - Environmental dependency - SFR calibrations - IMF variations - Secular processes, high resolution dynamics - Aperture corrections for other surveys	- SMBH - Kinematics and stellar populations - Interacting galaxies - star formation	- Kinematics classification - ISM properties - SP in outskirt, SF vs radial migration - SP gradients, age and metallicity - Galaxy assembly	- Galaxy morphological transformation - Mass and angular momentum assembly - Gas feeding and feedback	- Accretion - Formation of bulges and ellipticals - Quenched SF in groups and clusters - Stellar, gas, dark matter, mass assembly	- Clustering of SF evolution in time - Stellar cluster formation - SFH effects on UV calibration - Environmental effects - Supernovae surrounding

D Semester 2018B Observing Plan

For 2018B, we have a wide variety of targets to observe. Depending on the allocated time and the position of the SITELLE runs across the semester, we will prepare the phase 2 observations. Within our target list, we have some flexibility for the selection of the observed sampled in order to reach our scientific goals. We have targets of different metallicities, stellar densities, neutral gas densities, SFR, SFE, and different galactic structures (here mentioned in their order of priority for the survey) from the data already observed. The number of regions we have for each environment category will grow progressively as the data are reduced and observing priorities are adjusted accordingly. As a first step, we want to focus on galaxies with a prominent bulge, in order to study HII regions within high stellar density areas, and on targets with HII regions susceptible of having a very low metallicity, as often seen in massive spiral outskirts or in much less massive objects. The first observations in 2018B will therefore focus on T 2-4 and T 8-9 (see Fig. 19. The first priorities will be NGC 6946 (SN1 only), M 77, NGC 2903, NGC 4151, UGC 12632, NGC 337A, UGC 5829, UGC 7698. Therefore, a first SITELLE run could start later in the semester (e.g. early October) and a second run would be useful around the end of December and the beginning of January.

E Discussion on the Program Robustness

SIGNALS is a long term project that is viable by itself. It does not depend on other proposals, although it will benefit from synergy with other surveys and data already available. The priority of the observation sequence is defined by three aspects: 1) completing observations on a given field with the three filters when possible, 2) make good use of the grey/dark time period with respect to the filters observational constraints, and 3) observe targets that are most valuable for the optimal completion of the science goals. The rate of acquisition of the data does not impact the program as long as it is completed during the eight semesters. SITELLE performance has improved since its commissioning, and usual variations in modulation efficiency ($\sim$5%) will not impact our project. The flexibility of our sample makes SIGNALS a perfect program to match with any other large programs that could be accepted for the same period. We can easily adapt to the fact that the observing rate will increase with time as it will give our team some time to work on the first data set and improve our analysis method.

The SIGNALS collaboration is composed of an interdisciplinary team of expertise covering many fields of extragalactic astrophysics. The project does not stand on the shoulders of one person and several team members have experience with large projects, complex data management, and observational strategies. SIGNALS is a very competitive program and other research teams are planning to replicate it in the far future (ex: SDSS-V Local Volume Mapper). Only CFHT offers the instrumental capabilities of making SIGNALS a reality in the next years to come.

F Data Management Plan

F.1 Proposed Proprietary Period

For SIGNALS, we suggest to keep the usual proprietary period for Large Program:
- Participating community access : All members of a community participating in a LP (i.e. allocating observing time to the LP) will have immediate access to the data through the CADC. PI may give access to international collaborators.
- World Access : The default is one year proprietary period after the end of each semester for the duration of the LP.

F.2 Real-time Analysis Requirements

There is no need for real-time analysis with SIGNALS. All data cubes will be reduced with ORBS, the fully parallelized code first developed by T. Martin for SpIOMM and SITELLE, and now operated by CFHT.. ORBS provides astrometric, photometric, and wavelength calibration for all pixels in the FOV. Emission lines flux, width, centroid, and continuum level are optimally extracted with ORCS, a software also provided by T. Martin to accurately fit the peculiar line profiles characteristic of an IFTS (namely symmetric cardinal sine functions when expressed in terms of wave numbers). An example of the fit of an HII region spectrum is shown in Figure 14 for the filters SN1, SN2, and SN3, at a lower-spectral resolution than the one required for in SIGNALS.

F.3 Data Analysis Plan and Available Resources

Our team has plenty of experience in the analysis of 3D spectroscopy from the use of SpIOMM, SITELLE, PPAK instrument (within the CALIFA survey), ALMA, and MUSE. Experts in the modeling of HII regions will work on the development of adapted tools for the SITELLE dataset analysis, including a large database of models required for future comparisons. The dynamical aspect of the survey will be in good hands, as many team members are focusing their interest on the detailed study of velocity fields. Many collaborators have expertise in stellar population models, a central element for the IMF investigation.

Figure 15 presents the diverse processing steps from the observation to the extraction of the physical parameters. Data products will be distributed to the collaborators and the communities from the SIGNALS' WEBSITE. Figure 18 shows the different working teams within the SIGNALS collaboration along with their designated coordinators. It also includes an overview of each team's responsibilities during the data processing and analysis part of the project.

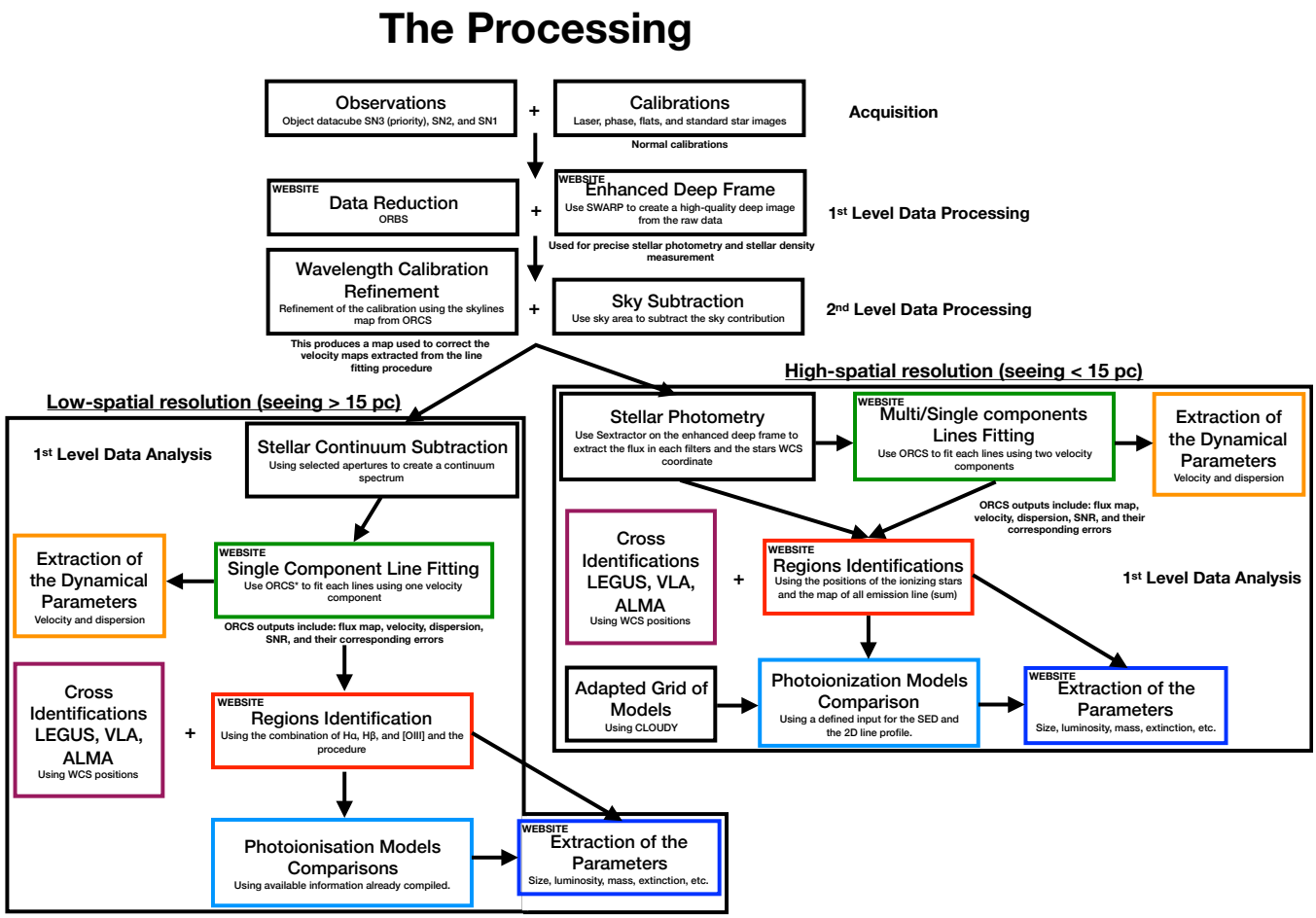

Figure 15: Organigram of the data processing. Note that all items with the mention WEBSITE will be accessible for every member of the team from the SIGNALS WEBSITE (http://www.signal-survey.org). Nine members of the SIGNALS collaboration are in the database management work team that is responsible for the data distribution from the WEBSITE (see Fig. 18).

F.4 List of Targets

Figures 16 and 17 present the RA distribution of the fields for the primary and secondary targets (some targets have more than one field) and the distance distribution for the primary targets as a function of their type. We have 39 primary targets (from which 33 fields will be selected for a total of 50 nights). The secondary target list contains 13 additional galaxies. The purpose of this list of objects is to facilitate scheduling while mildly relaxing the selection criteria (for example, the inclination of an irregular galaxy). A CVS file was uploaded with the complete list of targets (primary and secondary) and the number of fields.

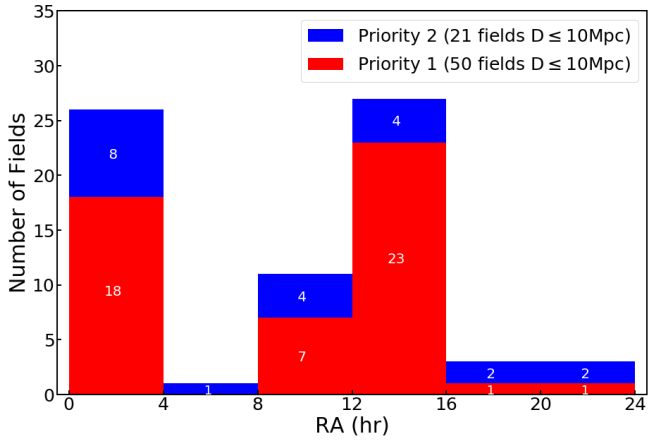

Figure 16: Distribution of the fields as a function of right ascension. There are 39 targets in our first priority list, some of which require more than one field.

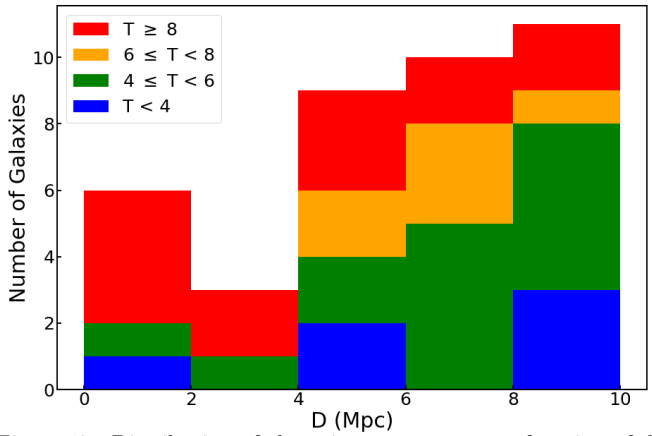

Figure 17: Distribution of the primary targets as a function of distance. The galaxies are color-coded according to their morphological type as given by the Hubble parameter T.

The Science

2nd Level Data Analysis

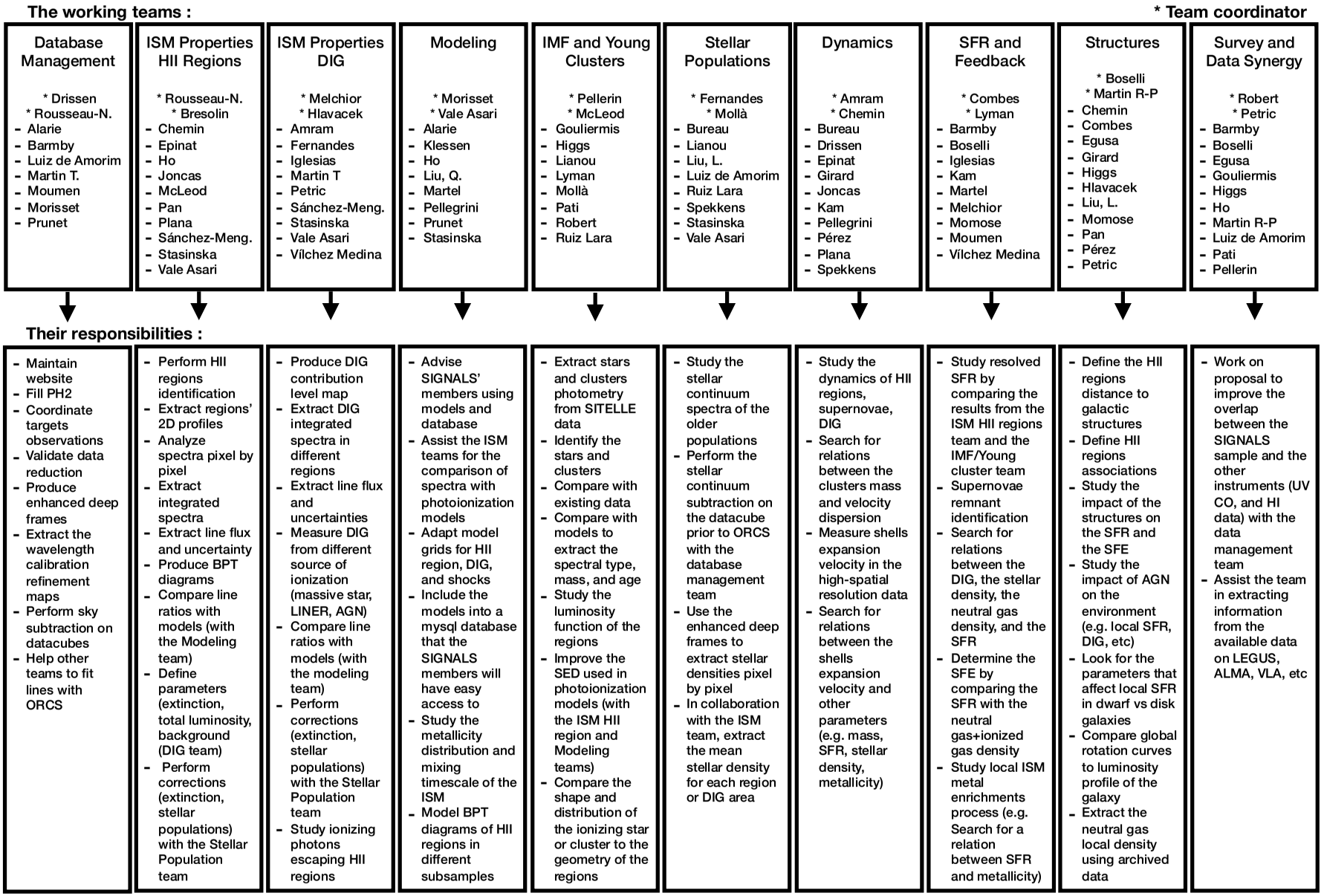

Figure 18: Working groups for the data analysis. Presentation of the work teams, their coordinators, and main responsibilities.

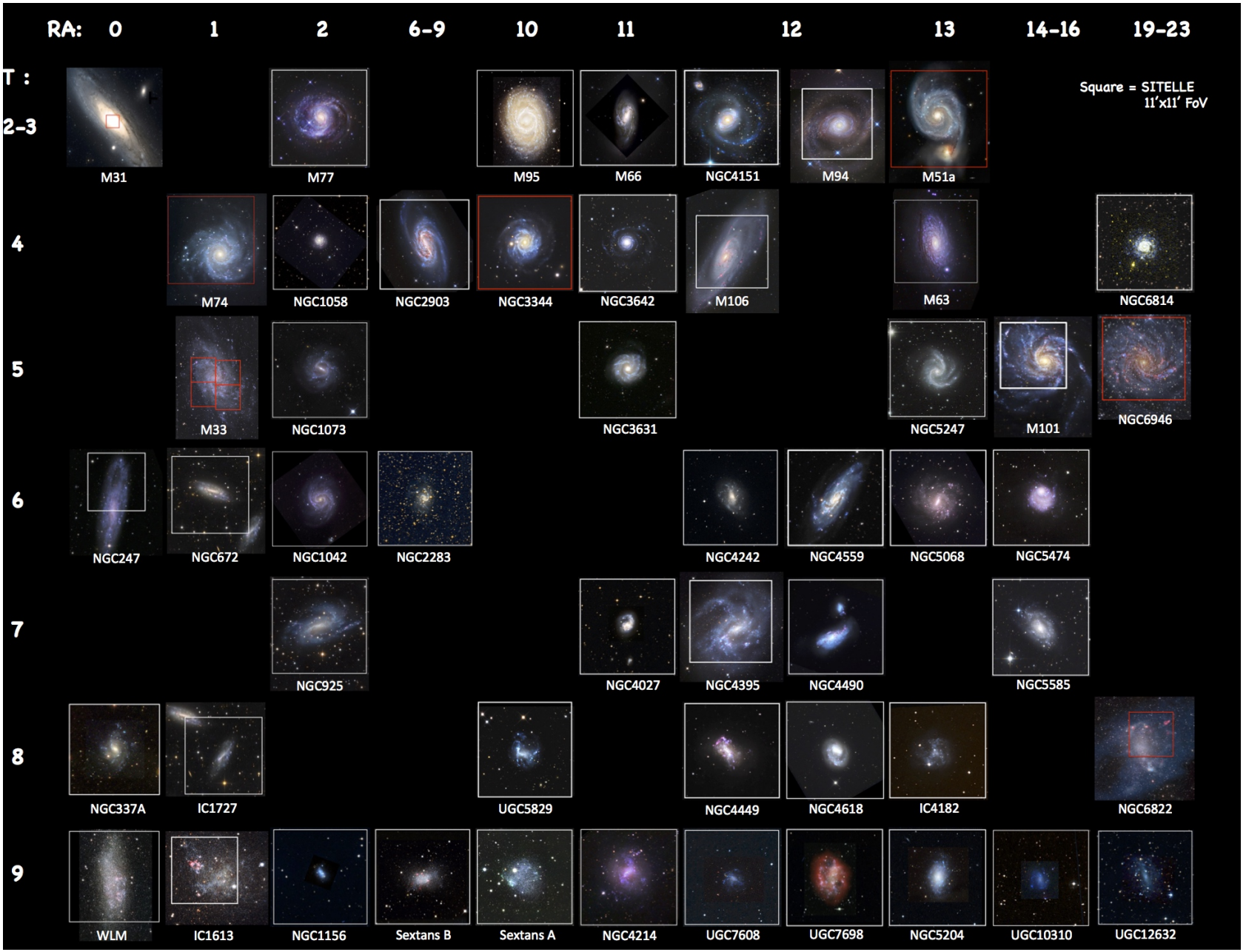

Figure 19: SIGNALS sample as a function of Hubble type and right ascension. The white squares show the size of SITELLE's field, but don't correspond necessarily to the selected FOV. Some targets are covered using more than one field (e.g. M 101 with four FOV). The red squares correspond to FOV on the galaxies already observed.

G Analysis of the Impact of the Optical Distortion

The optical distortion at the edge of the SITELLE's FOV will not affect significantly our science. This distortion can be measured on the PSF of the stars and does not impact the photometric calibration. Figure 20 shows the PSF measurements over SITELLE's FOV. The distortion is noticeable only in the corners (∼25% of the FOV). For most targets, the corners are used for sky sampling. Only a few fields selected for SIGNALS (about 10% of the fields) include HII regions that fall in the corners of the detectors. Among the field affected by the distortion, we estimate that only a small fraction of the HII regions sampled (from 0 to 10%) will fall on the corners (e.g. 1% for NGC 628 and ∼ 15% for M 33). HII regions falling in the area where the distortion is the worst (in the very corners where the PSF degradation is >25%) will only suffer from a degradation of their spatial resolution and an additional error (0.2″) on their position (RA, DEC). This corresponds to a negligible fraction of the HII regions included in the survey and we could still use these regions for most of the analysis.

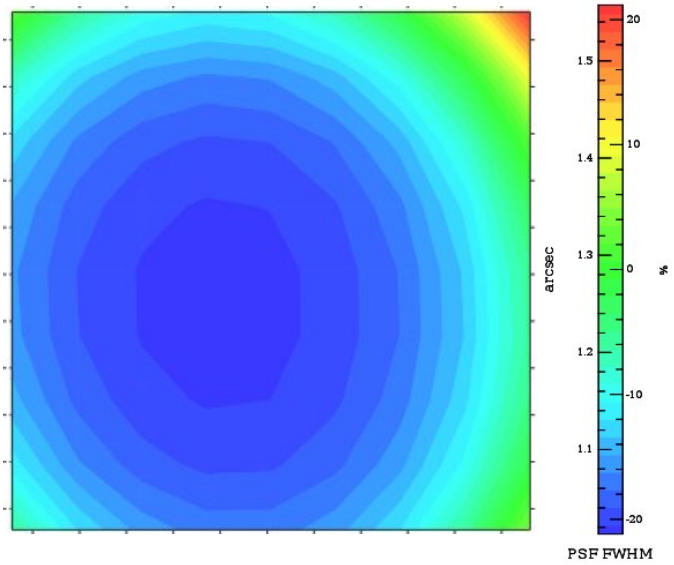

Figure 20: PSF measurements using the PSFEX code from ASTROMATIC on a crowded field of stars obtained from the stacked SN3 datacube of NGC 6822.

H SIGNALS Collaboration Team

PI Laurie Rousseau-Nepton (CANADA - CFHT)
Co-PI René Pierre Martin (HAWAII - U. Hawaii Hilo)
Co-PI Philippe Amram (FRANCE - LAM)
Co-PI Carmelle Robert (CANADA - U. Laval)
Co-PI Laurent Drissen (CANADA - U. Laval)
Alexandre Alarie (MEXICO - IA-UNAM)
Pauline Barmby (CANADA - U. W. Ontario)
Alessandro Boselli (FRANCE - LAM)
Fabio Bresolin (HAWAII -U. Hawaii Manoa, IfA)
Martin Bureau (UNITED KINGDOM - U. Oxford)
Laurent Chemin (CHILI - U. Antofagasta)
Roberto Cid Fernandes (BRAZIL - UFSC)
Françoise Combes (FRANCE - Obs. Paris)
Fumi Egusa (JAPAN - NAOJ)
Benoit Epinat (FRANCE - LAM)
Marianne Girard (SWITZERLAND - Obs. Geneva)
Dimitrios Gouliermis (GERMANY - U. Heidelberg)
Clare Higgs (CANADA - U. Victoria)
Julie Hlavacek-Larrondo (CANADA - U. Montréal)
I-Ting Ho (GERMANY - Max Planck Institute)
Jorge Iglesias (SPAIN - I. A. Andaloucía)
Gilles Joncas (CANADA - U. Laval)
Zacharie Kam Sié (CANADA - U. Montréal)
Prime Karera (CANADA - U. Laval)
Ralf Klessen (GERMANY - U. Heidelberg)
Victor Francisco Ksoll (GERMANY - U. Heidelberg)
Sophia Lianou (FRANCE - CEA Saclay)
Lijie Liu (UNITED KINGDOM - U. Oxford)
Qing Liu (CHINA - USTC)
André Luiz de Amorim (BRAZIL - UFSC)
Joseph Lyman (UNITED KINGDOM - U. Warwick)
Hugo Martel (CANADA - U. Laval)
Thomas Martin (CANADA - U. Laval)
Anna McLeod (NEW-ZEALAND - U. Canterbury)
Anne-Laure Melchior (FRANCE - Obs. Paris)
Maria Mercedes Molla Lorente (SPAIN - CIEMAT)
Rieko Momose (JAPAN - UN. Tsing Hua)
Christophe Morisset (MEXICO - IA-UNAM)
Ismaël Moumen (CANADA - CFHT, U. Laval)
Hsi-An Pan (TAIWAN - I.A. Sinica)
Ashok Kumar Pati (INDIA - IIAP)
Eric Pellegrini (GERMANY - U. Heidelberg)
Anne Pellerin (CANADA - SUNY)
Isabel Pérez (SPAIN - U. Granada)
Andreea Petric (HAWAII - IfA/CFHT)
Henri Michel Pierre Plana (BRAZIL - UESC)
Simon Prunet (FRANCE - CFHT)
Daniel Rahner (GERMANY - U. Heidelberg)
Tomás Ruiz Lara (SPAIN - IAC)
Laura Sánchez-Menguiano (SPAIN - U. Granada)
Kristine Spekkens (CANADA - RMC)
Grazyna Stasinska (FRANCE - Obs. Paris)
Marianne Takamiya (HAWAII - U. Hawaii Hilo)
Natalia Vale Asari (BRAZIL - UFSC)
José Manuel Vílchez Medina (SPAIN - I. A. Andaloucía)

Time Allocation Distribution

The time allocation distribution for SIGNALS calculated considering 50 nights of telescope time and the relative scientific contributions of the researchers from the multiple agencies involved (see Tab. 4). Following the advice of an executive member, the 50 nights have been divided in two blocks over the main agencies, Canada (31∼nights) and France (19∼nights). A small fraction of the time is also requested to Hawaii (3.6 nights), Taiwan (0.9 night), and China (0.2 night). The total is greater than 50 nights, but by doing so, the project's eligibility as an LP does not depend on the participation of all the agencies. We really want this project to be inclusive and hope that all the agencies will be participating. The contribution requested from Taiwan and China is mostly symbolic (corresponding to 0.113 and 0.025 night per semester). By contributing, all agencies will ensure direct access to the data to their community. If the number of nights accepted by the TACs is greater than 50, we will make good use of the additional nights available since the sample already includes additional targets.

Table 4: Time allocation distribution

Agency	Members	Time requested	Logic of the calculation
Canada	13	31 nights	CAN / (CAN + FR) × 50
France	8	19 nights	FR / (CAN + FR) × 50
Hawaii	4	3.6 nights	HI / All SIGNALS (55) × 50
Taiwan	1	0.9 night	TW / All SIGNALS (55) × 50
China	1*	0.2 nights	symbolic contribution

* 1 PhD student

Table 5 presents a scenario for the distribution of the time within each semesters for SIGNALS, taking into account the time available for all the LPs. We would not be affected by a fluctuation of the data acquisition rate. Following this allocation time scenario, we would received data regularly and be able to work in a continuous manner every semester.

Table 5: Time allocation distribution

Semester	LP Call # Nights	SIGNALS ∼ # Nights
2018A	–	–
2018B	29	±4
2019A	38	±5
2019B	50	±6
2020A	43	±5
2020B	55	±6
2021A	50	±6
2021B	68	±9
2022A	67	±9
2022B	–	–